DMPA-containing carbazole-based hole transporting materials for perovskite solar cells: recent advances and perspectives

Nicolas Berton, Rana Nakar, Bruno Schmaltz*

Laboratoire de Physico-Chimie des Matériaux et des Electrolytes pour l'Energie (PCM2E), Université de Tours, Parc de Grandmont, Tours 37200, France

* Corresponding author : bruno.schmaltz@univ-tours.fr

Abstract

Perovskite solar cells (PSC) based on metal-organic halide perovskites have emerged as one of the most promising photovoltaic technologies. Power conversion efficiency (PCE) has increased remarkably over the last few years from less than 10% up to certified efficiencies exceeding 23%. Selective interfacial layers play a critical role in charge extraction processes. In order to obtain high efficiencies, a hole transporting material (HTM) is required. Huge research efforts have been made to design efficient and low-cost materials. Carbazole-based HTMs are among the most promising new HTMs, in particular when they are substituted with dimethoxydiphenylamine (DMPA) units. This review gives an overview of the different classes of DMPA-containing carbazole-based HTMs and highlights the synthetic pathways, the structure-property relationship and the photovoltaic performances obtained in PSC devices. The relevance of structural variations and chemical doping processes is discussed with regard to efficiency and stability issues.

Keywords: perovskite solar cell, hole transporting material, carbazole, DMPA, HTM

I. Introduction

Emerging photovoltaic (PV) technologies are attracting considerable attention due to the fact that solar energy is by far the most widely available source of renewable energy. Initially studied by Mitzi *et al.* for their opto-electronic properties,[1] metal-organic halide perovskites have made tremendous progress since the first report of perovskite in sensitized solar cells in 2009.[2] While fast perovskite dissolution in the liquid electrolyte prevented any practical use, the major

breakthrough that triggered most photovoltaic studies in the field was the fabrication in 2012 of a 9.7% efficient and durable solid-state perovskite solar cell (PSC) formed by spin-coating from a precursor solution.[3,4] Power conversion efficiency (PCE) of PSC has now skyrocketed up to 23.7%, far above other emerging technologies.[5–7] Therefore, PSC appears as the only photovoltaic technology that combines the prospect of scalable low-cost solution processing with high efficiency.

Today, the main hurdle towards industrial development remains the lack of stability and fast degradation of PSC due to light, heat, oxygen and moisture sensitivity. These issues could be addressed in part through perovskite compositional tuning, formation of a capping barrier layer on top of the perovskite, as well as encapsulation techniques.[8–14] It is also well established that interface layers play a critical role in charge extraction and stability in PSC.[15,16] In particular, a hole transport layer is required, and as in solid-state dye-sensitized solar cells (DSSC), spiro-OMeTAD (2,2',7,7'-tetrakis-(N,N-di-paramethoxyphenylamine)-9,9'-spirobifluorene) has become the standard hole-transporting material (HTM) that is used to build most efficient perovskite PV devices.[17–20] However, spiro-OMeTAD is not a viable HTM for large-scale applications due to its complex chemical synthesis and its prohibitive cost.[21] Furthermore, the use of spiro-OMeTAD raises stability issues related to its tendency to recrystallize and the migration of additives upon heating in operating devices.[22–24] Developing efficient, stable and low-cost alternatives to spiro-OMeTAD is therefore mandatory. Many research efforts have been dedicated to the design and testing of new HTMs over the past few years, including a vast majority of organic polymers and small molecules as well as a few inorganic materials such as CuSCN.[25] Recent review articles can be found, focusing on chemical structure variations or more specifically on dopant-free HTMs.[26–28] Organic molecules enable easy and precise tuning of energy levels and thermal properties through molecular engineering as well as low-temperature solution processing. Most small molecule HTMs incorporate the nitrogen-containing 4,4'-dimethoxydiphenylamine (DMPA) units. Nitrogen atoms are hole-acceptors and are introduced to enhance hole mobility. Meanwhile, it was evidenced that the electron-rich methoxy units play a role *via* passivation of defect sites on the perovskite crystal surface, thus improving both charge extraction at the perovskite/HTM interface and device stability.[29],[30] Along with a few families of HTMs including spirofluorene, [6],[31],[32] triphenylamine,[33],[34] truxene and triazatruxene derivatives,[35–37] carbazole-based HTMs are among the most studied and most promising. The

interest for DMPA-containing carbazoles as HTMs dates back to early works by Sellinger *et al.* and by our group demonstrating spiro-OMeTAD-competing performances in DSSCs when the carbazole was substituted with DMPA either in 3,6 (**CzP**) or 2,7 positions (**AS44**) (Scheme 1). [38–40]

Following those reports, DMPA-substituted carbazole derivates were first reported as HTMs in perovskite solar cells by Hagfeldt *et al.* in 2014. [41] Since then, a large number of studies have been published, accounting for several dozens of molecules. Given the many promising reports, we feel that it is time to review the advances and insights obtained with DMPA-substituted carbazole HTMs over the last 5 years and to assess how it provides guidelines for future design and processing of HTMs.

In this review, we will first classify the different DMPA-containing carbazole molecules and present the synthetic pathways available to afford them, before focusing on the physico-chemical, optoelectronic properties and photovoltaic behaviour (in PSC) of carbazole-based HTMs substituted with DMPA units in 3,6 (3,6CzDMPA) then 2,7 (2,7CzDMPA) positions. The relevance of further structural variations and chemical doping processes will also be discussed in line with efficiency and stability issues.

II. Synthesis

In the literature, the molecules based on 3,6CzDMPA moiety can be organized in three categories. The first class is constituted of mono-adduct molecules where the carbazole derivative is linked, by the 9 position of the carbazole, to an aryl or an alkyl group. For these kind of simple structures, the synthesis is usually done in three steps.[42] Starting from the cheap and commercially available carbazole, the first step consists in introducing the alkyl or aryl group on the 9 position of the carbazole. Then, using the reactive 3 and 6 positions, halogens (generally bromine or iodine) are introduced with yield between 85% and 93%. The final reaction is a Buchwald reaction in order to insert the DMPA units.

The second and third classes are constituted of more complex molecular structures, meaning with more than one 3,6CzDMPA unit. In these structures, the carbazole derivative moieties are linked to a multifunctional spacer which will also be called core. In the second class of hole conducting materials, the core consists of an aryl or an alkyl group (**Q221**, **dly-1**, **TCz-C3**). [41,43] In the

third class of materials, the multifunctional core is a benzyl group.[44,45] The structures of both classes can be seen as pseudo-dendrimers (see Scheme 2). Indeed, these molecules can be described as an alkyl, aryl or benzyl core which is connected to a first generation of carbazole units, and then to a second generation of DMPA groups. As known in the literature, [46,47] two reaction schemes are available to prepare such dendrimers. The first one is a divergent synthesis which starts from the core and introduces the first, then the second generation of subunits. The second one is a convergent synthesis which is the opposite strategy of sequence of reactions. Concerning the preparation of the 3,6-carbazole based complex structures mentioned above, both routes have been used during the last years (see scheme 2).

The synthesis of the second class of HTMs, containing an aryl or alkyl spacer, is performed using the convergent strategy. The detailed synthetic pathway is represented in scheme 3a. This route consists in five reaction steps, starting with the cheap carbazole molecule, and can be reduced by one step if the commercially available 3,6-dibromo-9H-carbazole is used as starting material. In this convergent strategy, the protection and deprotection steps on the 9 position of the carbazole are mandatory in order to prevent side-reactions during the Buchwald coupling. Usually, protective groups like benzyl, tertbutoxycarbonyl or tosyl are introduced. In the halogenation step (introduction of iodine or bromine), the choice of the halogen does not play an important role since the yield of both reactions is more than acceptable (>85%). [41,48] The choice of this strategy is, in the case of the aryl spacer, driven by a solubility issue. Indeed, using the divergent strategy, one of the intermediates is the multi-halogenated aryl based molecule **1** (scheme 2), usually very slightly soluble in common solvents. The other argument in favour of the choice of this strategy is that the intermediate molecule **2** open up the synthesis of a wide range of materials in a single reaction step. The overall yield of this convergent synthetic route is 53% in 61 hours of reaction. [41] The growth of the number of new HTMs based on the N^3,N^3,N^6,N^6-tetrakis(4-methoxyphenyl)- carbazole3,6-diamine (intermediate **2**) has created a niche market and a company, such as Ikamba Organics (France),[49] is already selling this intermediate.

In the literature, the strategy which was adopted for the synthesis of the third class of HTMs is the divergent strategy. Indeed, the flexibility brought by the benzyl derivative core **3** discards the solubility problems of the intermediate **1**. The reaction scheme of the synthesis of this third class of HTMs is presented in figure 3b. Since this route no longer needs protection/deprotection

reactions, the final compound can be obtained in just three steps. Furthermore, the "click" reaction to afford intermediate **4** with high yield (>85%) [44] strengthens the choice of this route. Nevertheless, this strategy shows some limitations when discussing the last reaction yield. Although the latter is acceptable when at most 4 DMPA units are introduced (**V886**, **V911**, **V885**) (>65-70%), the yield of the octa-Buchwald reaction (**V957**) does not exceed 50%. That is why the convergent or divergent strategy might be reconsidered depending on the number of carbazole derivative moieties (intermediate **2**) introduced in the final molecule.

In the literature, N^2,N^2,N^7,N^7-tetrakis(4-methoxyphenyl)-*9H*-carbazole-2,7-diamine have also been synthesized for perovskite solar cell applications. For the same reasons previously described, the molecules have been synthesized following convergent [50–52] or divergent strategy. [44] The commercially available 2,7-dibromo-9H-carbazole is used and indeed reduces the number of reaction steps compared with the 3,6 analogue. Reducing the number of reaction steps does not always mean that the cost of the final molecule is cheaper. Nevertheless, in recent years, a scientific effort has been made in this direction to try to reduce the price of the HTMs. Although spiro-OMeTAD is still the reference as HTM in perovskite solar cells, the scientific community has become aware of the cost of some constituents of the cell. In order to reduce the price of the molecular glass, replacing the spirobifluorene core by a carbazole core is smartly thought. Based on this premise, a lot of work has been done to decrease the price of the carbazole derivative, introducing phenyl [53] (142.47 €/g), benzothiadiazole (43 US$/g) [54] or phenothiazin [55] (15 $/g) subunits on the 9 position of the intermediate **2**. Therefore, the cost of these molecules suffers from the use of expensive palladium catalysts, particularly when Buchwald coupling is used to graft aryl groups. Recently, Huang *et al.* connected two molecules of the intermediate **2** by using a simple oxidative coupling with $KMnO_4$ (**3,6 BCz-OMeTAD** and **2,7 BCz-OMeTAD**).[56] The cost of the 3,6 derivative decreases to less than 9 dollars per gram. Compared to the 2,7 analogous, the price of the 3,6 carbazole HTMs is always cheaper (by almost half). [56]

III. HTMs based on 3,6CzDMPA

1. Physico-chemical properties of 3,6CzDMPA based HTMs

When designing a new molecule, the target properties are of prime interest. In order to design a new hole transporting material for perovskite solar cells, some thermal and electronic properties should be taken into account. Table 1 summarizes the main properties of this series of materials.

In the following section, we will try to show the relation existing between the chemical structure of the HTMs and their properties. Some orientations will be given in order to understand the design of the materials.

The thermal properties gather the determination of the degradation temperature (Td) and the glass transition temperature (Tg) (or the melting temperature in some rare cases). Usually, the materials based on dimethoxydiphenylamine carbazole (CzDMPA) units have molecular glass behaviour, which means that no crystallization temperature is observed in DSC experiments. In perovskite solar cells, the Tg should not be too low, to prevent the melting of the HTMs during illumination. The standard HTM material is spiro-OMeTAD and its Tg is 120°C. [57] One can note that a higher glass transition temperature is more favorable for the encapsulation process of the cell. The Tg can be controlled by the grafting of substituents on to the 9 position of the carbazole unit, and two main parameters play a role : the nature of the spacer (core) and the dimensionality of the final molecule. The dimensionality can be defined by the number of carbazole units connected to the spacer. When the spacer is an aryl group, the glass transition temperature generally exceeds 100°C. If the substituent is a phenyl group, Tg is 97°C and increases, for example, to 109°C with a dithieno[3,2-b:2',3'-d]pyrrole unit (**M112**) [55] or even to 130°C with a phenothiazine unit (**M114**). [55] On the other hand, when alkyl chains are connected to the CzDMPA, the more extended the chain, the lower the Tg. For example, the Tg of **B63** with an ethyl group [58,59] is 25°C higher than **B58** with a hexyl chain (80°C vs. 55°C). As previously mentioned, the dimensionality plays a role. The Tg of **TCz-C6** [43] is 66°C showing that the connection of a second CzDMPA moiety, increasing the dimensionality, increases the Tg too. Then, this value can be controlled by increasing (**TCz-C12**, 47°C) or decreasing the spacer chain length (**TCz-C3**, 107°C). The aryl spacer follows the same trend and an increase of the Tg is observed for **vm-2** compared with **X51**, respectively 186°C and 153°C. [60] Of course, if alkyl chains are introduced on the aryl core (**vm-3**), the temperature decreases to 124°C. Xue *et al.* studied a binaphtol derivative spacer and showed that this latter group increases the Tg to 188°C (**Q205**) compared with phenyl analogues (**HBZ-70**, 168°C). [61,62] Additional phenyl rings can even be added to the binaphtol core and increase even more the glass transition temperature to 198°C (**Q221**). [63] On the contrary, additional alkyl chains decrease the Tg to 128°C (**Q222**). [63] The introduction of fluorine atoms on to the aryl spacer has also been studied. Zhu *et al.* studied HTMs where the spacer between the two CzDMPA moieties is constituted of a benzothiadiazole (BTZ) unit (**JY5-**

7). [54,64] They showed that the introduction of fluorine atoms on the BTZ moiety decreases the Tg from 165°C without fluorine atom (**JY5**) to 134°C for HTM possessing two fluorine atoms (**JY7**). The same tendency has been observed on mono-adducts (**CzP**, **CzPF**).[53] As we have already noted, the dimensionality of the structure increases the Tg. For example, tri-adducts such as **BTT-2**, **SGT-405(3,6)** or **3,6Cz-TPA** reached high Tg with respectively 216°C, 193°C and 146°C. [65–67] Getautis *et al.* studied benzyl spacers with two to four CzDMPA moieties and showed that neither the grafted positions **V886** (ortho-), **V885** (meta-) or **V911** (para-))[44] nor an additional phenyl unit (**V997**)[68] influenced the Tg (139-141°C). Therefore, additional CzDMPA moieties increase the rigidity of the structure and so increase the glass transition temperature to 160°C (**V1039**, **V957**). [44]

The decomposition temperature (5%wt loss) measured by TGA is useful to confirm the stability of the molecules upon solar illumination. In the whole literature, CzDMPA based molecules are stable over 300°C, which is suitable for solar cells. Usually, the more the spacer is aryl constituted, the more the HTMs are stable, reaching T_D exceeding 400°C.[45,55,67]

When designing a HTM, another significant parameter which should be considered is the charge transport properties. High mobility is beneficial to the balance of the charge transport in PSCs. One of the reasons why the potential of the standard material, spiro-OMeTAD, is limited for up-scaling in applications like PSCs or even DSSCs is its low charge carrier mobility. Although the development of a new generation of HTMs with high charge carrier mobility is of high priority, up to now, few carbazole based materials overcome the transport properties of the spiro-OMeTAD. In the literature, three different methods are usually able to determine the hole mobility. Most of the time, space-charge-limited current (SCLC) is used in hole-only configuration. This technique allows the measurement of the charge carrier mobility of pristine or doped HTMs. In doped state, spiro-OMeTAD shows a mobility of 2.10^{-4} $cm^2.V^{-1}.s^{-1}$ (ITO/PEDOT-PSS/Spiro-OMeTAD/MoO_3/Al configuration) [50] and a value of 8.10^{-5} $cm^2.V^{-1}.s^{-1}$ in pristine state.[55,56] Xue *et al.* showed that adding phenothiazine (PTZ) or dithienopyrrole (DTP) moieties on the 9-position of the CzDMPA allows the control of the charge carrier mobility. Even if the combination of the carbazole building block and PTZ (**M111**) outperforms its analogue with DTP (**M112**), the values, although close to the reference material, stay lower.[55] Zhu *et al.* used a tetraphenylethylene spacer to synthesize **W3** and **W4**.[50] Although the di-adduct **W3** shows low

solubility, the hole mobility of the tetra-adduct **W4** reached, in doped state, $1.35.10^{-4}$ $cm^2.V^{-1}.s^{-1}$. Among the materials using a conjugated aryl derivative linker, **X51** and **X19** could overtake spiro-OMeTAD transport properties with respectively $1.19.10^{-4}$ and $1.51.10^{-4}$ $cm^2.V^{-1}.s^{-1}$ in doped films.[41] Driven by these results, Zhu *et al*. developed molecular glasses where the biphenyl spacer has been modified by adding benzothiadiazole derivatives (**JY5**, **JY6**, **JY7**) or by introducing nitrogen atoms (bipyridine spacer).[64,69] The SCLC measurements, in undoped as well as doped films, indicate values 2 to 4 times higher than spiro-OMeTAD in the same conditions. Since the carbazole based molecules possess a molecular glass behaviour, an anisotropic charge transport can be expected. Organic Field Effect Transistors (OFET) have also been used to measure the transport properties in the solid state. Nevertheless, even if their mobility values are close to the reference material, the highest value is 7.10^{-6} $cm^2.V^{-1}.s^{-1}$ for **3,6Cz-TPA**.[67] The third method which has been utilized in the literature to measure the hole-drift mobility is xerographic time-of-flight (XTOF). The results are usually given at weak and at high electric field ($6.4.10^5$ $V.cm^{-1}$). Concerning spiro-OMeTAD, the measured mobility is 4.10^{-5} and 5.10^{-4} $cm^2.V^{-1}.s^{-1}$ at weak and high electrical field, respectively. Snaith *et al*., who developed the benzyl spacer HTM series (**V886** to **V1061**), show that the transport properties are basically getting close to the spiro-OMeTAD, which is encouraging in order to design new molecular glasses.[44,45,70] Therefore, the authors calculated the dipole moment of **V911** and **V885** (DFT calculation) and show that better hole drift mobility values, compared with spiro-OMeTAD, could be reached.[44] They suggest that intramolecular interactions take place in the HTM with methoxy groups, probably due to the hydrogen bonding formation.[71]

The energetic properties of the HTMs and more particularly the energy levels should be taken into account in the design of the target molecules. In order to transfer the electron to the perovskite, the HTMs must have a Highest Occupied Molecular Orbital (HOMO) higher than that of the perovskite (higher than 5.44 eV for $CH_3NH_3PbI_3$). In the literature, it is quite difficult to give a trend of appropriate materials since the value of the reference spiro-OMeTAD is completely different depending on the measurement techniques or the research groups. For example, using photoelectron spectroscopy in air (PESA) or cyclic voltammetry (CV) techniques, 5.00eV (PESA)[72], 5.15eV (PESA),[73] 4.70eV (CV)[74] or 5.22eV (CV)[75] can be found. Zhu *et al.* studied the introduction of acceptor units in the biphenyl spacer (**JY5**, **JY6**, **JY7**) and showed that the HOMO level of the HTMs is not significantly modified compared with the original molecule

(**X51**).[54,64] Nevertheless, the band gaps of the D-A materials decrease from 2.93eV (**X51**) to approximately 2.30eV. Usually, the whole CzDMPA based HTMs are well suited for electron transfer to the perovskite.

Finally, it is known in the literature that the improvement of the water resistance of either the HTM molecules or the additive is a useful strategy for enhancing the device stability.[76,77] Contact angles of a water droplet on doped HTM films have been measured. Usually, the CzDMPA based HTMs show an increase of the contact angle compared with doped spiro-OMeTAD film. Contact angles for the **M111-M114** series (71.5-81.1°) were all reported to higher than the spiro-OMeTAD (68.8°).[55] Zhu *et al.* studied the water resistivity of **JY5** [64], **F22**, **F33** and **X51**[69] and showed that the synthesized molecules are more hydrophobic (77-87° compared with 74.5° on spiro-OMeTAD) and could more effectively prevent water diffusion into devices, which could also account for good device stability.

2. Photovoltaic performances of HTMs based on 3,6CzDMPA in PSC

Perovskites have the generic chemical formula ABX_3, where A is a cation, B a dication, and X is an anion. Perovskite materials used in PSCs are usually 3-dimensional lead (Pb^{2+})-containing metal-organic halide perovskites where A is an organic cation such as methylammonium (MA) or formamidinium (FA). $MAPbI_3$ has been widely used so far, but the optoelectronic properties and the stability of the perovskite layer can be further adjusted by compositional tuning of mixed-cation and/or mixed-anion perovskites. PSCs can be built in a conventional n-i-p or inverted p-i-n device configuration with either a planar or mesoporous structure, depending on the nature of the bottom interface on which the perovskite layer is deposited (Figure 1). Regardless of the device architecture, both n-type and p-type interfaces play a key role in selective extraction of electrons and holes, respectively. To date, most organic HTMs have been used in conventional PSCs. However, the diversity of perovskite composition, device structure, electron transport layer (ETL) materials as well as various HTM additives and dopants used in PSCs often makes it difficult to compare the photovoltaic behaviour of the different HTMs reported in the literature. Besides, and adding to this difficulty, some disparity in the degree of purity between the various synthesized HTMs cannot be excluded. Little attention has been paid to the HTM purity level in PSC, although insufficient purity of the organic compounds is known to negatively influence PV performances in organic photovoltaics and in solid state DSSCs. [78] The J-V characteristics of PSCs containing

3,6-DMPA-substituted carbazole HTMs are summarized in Table 2. The PCE of the reference PSC fabricated with spiro-OMeTAD is also indicated for the purpose of comparison. One should keep in mind that record PSC efficiency has roughly doubled since the first works on carbazole-based HTMs in 2014. Thus, the PCE of the reference cells in Table 2 cover a wide range from approximately 10 to almost 20%.

The mono-adduct HTMs functionalized on the nitrogen atom in position 9 (*N*) of the carbazole moiety constitute the first class of 3,6CzDMPA materials that have been tested in PSC. Within this family, the *N*-alkyl and *N*-benzyl functionalized HTMs **B58**, **B73** and **V990/B63** (Scheme 4), suffering from low hole mobility and glass transition temperature, perform poorly.[44,58] The PCE of PSCs made with **V990/B63** reaches 5.02% in mixed cation mixed halide solar cells, and 10.8% in $MAPbI_3$ solar cells, but with strong hysteresis.

The *N*-aryl functionalized HTMs **X19**, **CzP** and **CzPF**, on the contrary, exhibit promising performances with PCE values close to those obtained with the reference spiro-OMeTAD HTM (up to 13.08% for **CzP** *vs* 13.45% for spiro-OMeTAD), in line with the good behaviour previously demonstrated for **CzP** in DSSCs.[41,53] Steady state and time-resolved photoluminescence (PL) measurements indicated improved charge transfer at the perovskite/HTM interface with **CzP** and **CzPF** compared with spiro-OMeTAD. In an effort to enhance the polarization of the molecule, 3,6CzDMPA was recently functionalized with more electron-accepting units (dithieno[3,2-b:2′,3′-d]pyrrole in the case of HTMs **M111** and **M112**, and phenothiazine for **M113** and **M114**). [55] The phenothiazine unit proved particularly promising. While the structure of **M113**, characterized by a strong dihedral angle, resulted in a limited internal charge transfer, **M111**, **M112** and **M114** present a strong donor-acceptor (D-A) character, with the LUMO of **M114** being located mainly on the phenothiazine. Enhanced hole mobility and conductivity as well as improved charge extraction at the perovskite/HTM interface can account for the high PCE of 17.17% measured with **M114** (18.07% PCE with spiro-OMeTAD).

The phosphonic acid-functionalized HTM **V1036** is kind of an exception among the mono-adduct 3,6CzDMPA molecules.[79] Designed for use in inverted p-i-n PSC, this molecule forms a dense self-assembled mixed monolayer (SAM) on ITO when combined with butyl phosphonic acid and enables PSC with 16.46% PCE and good stability when stored in the dark at room temperature and under nitrogen atmosphere.

The twin molecule **X51**, where a biphenyl group serves as a π–conjugated linker, was the first bis-adduct of 3,6CzDMPA to be reported.[41] Its promising PV behaviour, competing with spiro-OMeTAD (9.80% *vs* 10.20% PCE), has prompted chemists to design new derivates by tuning the properties of the core unit. HTM **HBZ-70** has a biphenyl core with methoxy substituents, whereas in **Q205**, **Q221** and **Q222**, binaphtyl cores with either methoxy, benzoxy or hexyloxy substituents are introduced, respectively. [61,62] All four HTMs present enhanced twisting compared with **X51**. In PSC, **Q221** has led to a PCE of 10.05%, similar to the reference spiro-OMeTAD. The bis-adduct **W3** reportedly suffered from poor solubility and could not be tested in perovskite devices. [50] HTM **BF-003**, having a dibenzofuran core, exhibits fair PV properties with a 14.07% PCE. [80] Recently, a HTM based on a pyrene core (HTM **dly-2**) demonstrated reduced charge recombination, high efficiency and enhanced stability under ambient conditions compared with spiro-OMeTAD (18.23 compared with 19.59% PCE). [81] A spirobisindane core was designed to lower the symmetry of the **Spiro-I** HTM. [82] A high PCE (18.57%) was obtained in small-area devices, competing well with spiro-OMeTAD devices (19.59%). The stability under ambient conditions was better than with spiro-OMeTAD, retaining 80% after 100 days. The PCE dropped considerably in 1 cm^2 devices but was found to be slightly higher than when using spiro-OMeTAD (9.78% *vs* 8.29%).

HTMs **V885**, **V886**, **V911**, **V997** and **V1061** constitute a family of twin molecules with a non-conjugated core.[44,45,68,70] Devices fabricated with these molecules exhibited better stability than spiro-OMeTAD devices when stored in the dark, and all molecules, with the exception of **V1061**, afford efficiencies that are very similar to spiro-OMeTAD. In particular, the grafting position on the phenyl ring (in *ortho*, *meta*, or *para* positions) does not seem to play a significant role, which can possibly be explained by the flexibility brought by the linker. It can be noticed that the **V908**, **V928** and **V931** analogues where methoxy groups are replaced by methyl exhibit lower conductivity and hence lower PCE below 17%. The FK209 dopant used in this case may not be appropriate for these HTMs.

Very promising donor-acceptor HTMs were also derived from the structure of **X51**. Introducing a central benzothiadiazole (BTD) acceptor unit between the phenyl units in HTM **JY5** leads to a strong efficiency improvement from 13.20 to 16.87% PCE, beyond the PCE measured using spiro-OMeTAD as reference (16.24%).[64] The efficiency was pushed even further up to 18.54% upon

mono-fluorination of the BTD unit in HTM **JY6**. [54] In the latter case, a remarkable fill factor of 0.81 was monitored. Instead, the difluorinated HTM **JY7** exhibited poor film-forming properties and hence a lower PCE of 15.71%. The second approach to build D-A HTMs consists in the replacement of the biphenyl core with a bipyridine one. HTMs **F22** and **F33** lead to excellent PCE of 17.71 and 18.48%, respectively, owing to high hole mobility and conductivity. [69] The higher PCE of **F33** was due to an improved V_{OC} (1.11 V), which can be related to a slightly lower HOMO level induced by the increased planarity, as suggested by DFT calculations.

The bicarbazole derivative **3,6 BCz-OMeTAD** is the last example of a 3,6 bis-adduct HTM. As will be discussed below, along with its 2,7 analogue, this HTM performs well as dopant-free HTM, demonstrating a 17.0% PCE and an interesting stability in the dark as well as under continuous illumination. [56] Interestingly, these results were obtained with 1 cm^2 devices.

The star-shaped HTMs **3,6-CzTPA**, **SGT-405(3,6)** and **BTT-2** based on a three-dimensional aromatic triphenylamine core and a planar aromatic phenyl or benzotrithiophene core respectively, all contain 3 CzDMPA groups. **3,6-CzTPA** has demonstrated up to 15.89% PCE, relatively close to that of spiro-OMeTAD (17.13%) in mixed cation mixed halide PSC,[65,67] whereas the efficiency of **BTT-2** is comparable with spiro-OMeTAD in a mixed halide PSC (17.5%), and **SGT-405(3,6)** outperforms it (18.87% *vs* 17.71%).[66] In particular, all three molecules afforded high short-circuit current density equal to or above 22 $mA.cm^{-2}$. Devices based on **SGT-405(3,6)** were also found to be more stable than those based on spiro-OMeTAD or on the 2,7 analogue **SGT-405**. HTMs **W4** and **dly-1** are tetra-functional molecules based on an aromatic core linker. [50,81] **W4** leads to 13.30 % PCE, approaching the performance of spiro-OMeTAD (15.01%). However, **W4** was found to be less efficicient than its 2,7 analogue **W2**, as discussed below (see the 2.7 section). The pyrene-based HTM **dly-1** exhibited a relatively high PCE (17.19%) but did not reach the efficiency obtained with spiro-OMeTAD (19.59%) nor using its twin analogue **dly-2**.

The branched HTMs **V1039** and **V1050** bearing three 3,6CzDMPA adducts and **V957** with four adducts all have flexible core linkers. [44,45] **V1039** and **V957**, having lower mobilities than their bifunctional homologues, give lower PCE, still approaching 17%. The fluorene-based HTM **V1050**, on the other hand, was shown to be competitive with spiro-OMeTAD, owing to high J_{SC} and fill factor, thus performing better than its bis-adduct homologue **V1061**.

IV. HTMs based on 2,7CzDMPA

Examples of 2,7-substituted carbazole-based HTMs (Scheme 5) are much less common than their 3,6 analogues, which can be easily understood when considering that their synthesis is more complex and leads to higher synthetic costs. For instance, the estimated cost of **2,7BCz-OMeTAD** is almost twice as high as **3,6BCz-OMeTAD** (8.55 $/g *vs.* 14.00 $/g). [56] On the other hand, the 2,7-linked carbazole moiety is more conjugated than its 3,6 counterpart, where charges can be trapped on the nitrogen atom of the carbazole.[83] Improved hole mobility and photovoltaic performances could therefore be expected with 2,7-carbazole derivatives, in a similar way to what was previously observed in organic photovoltaics. [84,85]

The properties and photovoltaic performances of the various reported 2,7-substituted HTMs are summarized in Table 3 and Table 4, respectively. The early report of molecules **SGT-404**, **SGT-405** and **SGT-407**, in 2014, demonstrated promising properties.[52] The alkoxy-functionalized biphenyl core of **SGT-404** resulted in relatively low T_g (70.5°C) and T_d (330°C), whereas **SGT-405** and **SGT-407** exhibited excellent thermal properties with T_g of 170°C and 200°C, respectively, and T_d beyond 400°C, owing to a rigid aromatic core and high molecular weight. Only the **SGT-405** HTM exhibited a semi-crystalline behaviour, the other two being amorphous. All three HTMs exhibited HOMO and LUMO energy levels comparable with spiro-OMeTAD. The three-armed HTMs performed better than the two-armed HTM, with 14.79%, 13.86% and 13.28% PCE for **SGT-405**, **SGT-407** and **SGT-404**, respectively (compared with 15.23% for spiro-OMeTAD). The efficiency was found to be related to the conductivity of the HTM. The PCE was later increased to 18.00 % using **SGT-405** in mixed anion PSC, comparable with cells based on spiro-OMeTAD (17.71%) and slightly lower than using the 3,6 analogue **SGT-405(3,6)** (18.87%).[66]

Two-armed HTMs with a rigid aromatic linker were also reported by Qiao *et al.* (HTMs **Q197** and **Q198**).[61] Both HTMs are amorphous and exhibit fair thermal properties, but the reported efficiencies are low (8.38% with **Q197** vs 8.73% with spiro-OMeTAD). In spite of a very low mobility, the disubstituted HTM **W1** with a tetraphenylethylene core affords 14.92% PCE, competing with spiro-OMeTAD (15.01%). However, the four-armed HTM **W2** gives much higher hole mobility (3.06×10^{-4} $cm^2.V^{-1}.s^{-1}$ from SCLC measurements of doped films in hole-only device configuration) and efficiency (16.74%), confirming the potential of dendrimer-like HTMs.[50]

Furthermore, device stability under nitrogen atmosphere was equivalent to that of spiro-OMeTAD-based devices.

The diphenylamine-based **V946** HTM recently published by Getautis, Nazeeruddin and co-workers is a twin-molecule with a non-conjugated aryl/alkyl core.[44] Its thermal behaviour (T_g 113°C and T_d 411°C) and hole mobility (6.05×10^{-4} $cm^2.V^{-1}.s^{-1}$ as measured by XTOF) are relatively good. **V946** leads to a high PCE of 17.02% in mixed-cation mixed-halide PSC, but does not outperform spiro-OMeTAD (18.79%).

The *N*,*N*'-bicarbazole-based **2,7 BCz-OMeTAD** [56] and the *N*-ethylhexyl-functionalized **CMO** (also known as **EH44**) [86,87] are the simplest 2,7 derivatives reported so far. They are also the only HTMs of the 2,7 family to be reported as dopant-free HTMs in PSCs. A 17.6% PCE was thus achieved with **2,7 BCz-OMeTAD**, close to that of doped spiro-OMeTAD (18.5%). Regarding the HTM **CMO/EH44**, a PCE of 15.92% was initially reported without dopant (comparing well with 16.70% for spiro-OMeTAD). The efficiency was further improved up to 18.50% upon doping optimization, as will be discussed below.

In spite of the limited number of studies, a few insights can be gained by comparing the 3,6 and 2,7-substituted HTMs. Comparison of the optical properties of 2,7- and 3,6-DMPA-substituted carbazole HTMs shows a blue-shifted absorption and a stronger photoluminescence intensity in the case of the 2,7 molecules, indicating a weaker charge transfer character because of the weaker electron-donating ability of the DMPA groups when substituted in 2,7 positions. However, this does not translate into a general rule regarding HOMO energy levels. It can be noticed that the 2,7 and 3,6 HTMs all have very similar HOMO levels. HOMO energy levels of **2,7 BCz-OMeTAD** and **Q197** are slightly lower than that of their 3,6 analogues **3,6 BCz-OMeTAD** and **Q205**, respectively, whereas **W1**, **W2** and **V946** exhibit the opposite trend when compared with **W3**, **W4** and **V886**, respectively. As suggested by density functional theory (DFT) calculations, these small variations may be governed in some cases by structure distortions induced by steric hindrance, which is stronger in the 2,7-substituted molecules.[50]

The degradation temperature of the 2,7 HTMs tends to be slightly better than that of their 3,6 counterparts (in particular, T_d = 442°C for **2,7 BCz-OMetAD** *vs* T_d = 397°C for **3,6 BCz-OMetAD** and T_d = 411°C for **V946** *vs* T_d = 390°C for **V886**). There is no obvious trend regarding the glass transition temperature, but the position of the substituents can induce significant variations.

Interestingly, T_g is strongly improved with **2,7 BCz-OMeTAD** (145°C) compared with that of **3,6 BCz-OMeTAD** (100°C) as well as with **SGT-407** (170.8°C) compared with that of **3,6Cz-TPA** (146°C). On the contrary, **V946** exhibits a lower T_g than **V886** (113°C *vs* 141°C, respectively), which could be related to differences in molecular interactions and ordering.

The few comparable data available regarding hole mobility do not highlight any significant influence of the 2,7 *vs* 3,6-substituted HTM structure. Indeed, hole mobility values are very close for **2,7 BCz-OMeTAD** and **3,6 BCz-OMeTAD** (0.95×10^{-4} $cm^2.V^{-1}.s^{-1}$ and 1.13×10^{-4} $cm^2.V^{-1}.s^{-1}$, respectively, from SCLC measurements) as well as for **V946** and **V886** (6.5×10^{-4} $cm^2.V^{-1}.s^{-1}$ and 6.0×10^{-4} $cm^2.V^{-1}.s^{-1}$, respectively, according to XTOF measurements at 6.4 10^5 $V.cm^{-1}$ field strength). It should be mentioned however that the hole mobility of doped **W3** measured by SCLC (3.06×10^{-4} $cm^2.V^{-1}.s^{-1}$) was more than double of that of doped **W4** thin films (1.35×10^{-4} $cm^2.V^{-1}.s^{-1}$).

Overall, the 2,7-substituted HTMs tend to slightly outperform the 3,6 homologues in terms of PV efficiency. **W2** gives a much higher PCE (16.74%) than **W4** (13.30%), which could be related in part to its higher mobility. Without dopant, **2,7 BCz-OMeTAD** also leads to higher PCE than **3,6 BCz-OMeTAD** (17.6% *vs* 17.0%), but steady-state efficiency of best performing devices is nearly identical. On the contrary, PSCs containing **V946** do not rival with **V886** (17.02% *vs* 18.45% PCE) despite higher conductivity. Finally, **Q197** (8.38%) performs better than **Q205** (6.51%), but device efficiencies were rather poor. More detailed studies on a wider library of molecules will clearly be necessary to confirm the generic trend. Perhaps more importantly, **2,7 BCz-OMeTAD**-based PSCs exhibit better long-term stability than **3,6 BCz-OMeTAD**-based PSCs without encapsulation under continuous 1 sun illumination in air, retaining up to 90% of initial efficiency (instead of 74%) after more than 2,000 hours. The origin of this improved stability is still unclear.

V. Structural variations based on CzDMPA

Among the CzDMPA based organic HTMs synthesized so far, some structure variations have been studied in PSCs (Scheme 6). Table 5 and Table 6 summarize respectively the thermal properties and mobility data, and the PV characteristics of PSCs based on HTMs. The low cost **Cz-OMeTAD**, synthesized in 3 steps with an overall yield of 70%, utilized both 3,6 and 1,8 reactive positions of the carbazole to introduce the DMPA moieties.[88] Even if the performance in PSC

planar architectures are still below the **spiro-OMeTAD** HTM, they are competitive with those of the costly reference (17.81% vs. 18.59%). Some extended core have also been studied. For example, **X25** and **LD22** possess an additional phenyl ring between the carbazole core and the DMPA, respectively grafted on the 3,6 and the 2,7 positions. Since **X25** shows interesting hole transport ($2.5.10^{-4}$ $S.cm^{-1}$), it exhibit a high PCE of 17.4% in a solar cell with mixed-ion perovskite $[HC\text{-}(NH_2)_2]_{0.85}(CH_3NH_3)_{0.15}Pb(I_{0.85}Br_{0.15})_3$.[89] For the 2,7-grafted version (**LD22**), the authors showed that the extension of the core increased the Tg (132°C).[90] But the interesting result lies in the good repeatability of the performance since they are independent of the doped HTM concentration. The PCE with doped HTM give a promising 17.18%, which is comparable with that of **spiro-OMeTAD** (17.73%). As previously mentioned, four reactive functions can be grafted on to the carbazole unit. Tang et al used the extended core and the four functions to synthesize **CZ-TA**.[91] The authors claimed that the HTM improve hole extraction and transport ($1.65.10^{-4}$ $cm^2.V^{-1}.s^{-1}$) to give a PCE of 18.28% in planar PSC with an impressive field factor of 81%. The same authors developed a thiomethyl containing analogous of **CZ-TA**, called **CZ-STA**.[92] They showed that switching the methoxy to a thiomethyl function downshifted the HOMO level and formed stronger Pb-S interactions with the perovskite, leading to better device performance. A binary HTM mixture consisting of 10 wt% **CZ-STA** and 90% **CZ-TA** achieved, in planar perovskite solar cells, a maximum power conversion efficiency of 19.85%. Ding et al have already tried the same approach and synthesized **CMT**, functionalized in 2,7 position.[93] This specific material has been used as dopant-free HTM in perovskite solar cells based on $CH_3NH_3PbI_3$ and achieved a PCE of 13.05% with a I_{sc} of 21 $mA.cm^{-2}$, an V_{oc} of 1.03V and a FF of 58%. Surprisingly, PSC based on doped **CMT** gave lower a performance (10.55%). In order to enhance the solubility of the HTMs in organic solvents, a flexible hexyloxy group have been introduced to afford **SGT-409**, **SGT-410**, **SGT-411**, and the 3,6 analogues **SGT-410(3,6)** and **SGT-411(3,6)**. [51,66] Therefore, moderate yields (11%-16.5%) have been reached. Finally, a macromolecule based on Cz-DMPA has been developed by free radical polymerization of vinyl monomer using AIBN.[94] **PVCz-OMeTAD** shows excellent film-forming ability, suitable energy level and high hole mobility ($3.44.10^{-4}$ $cm^2.V^{-1}.s^{-1}$). The non-conjugated polymer has been used in thin film, dopant-free perovskite solar cells (see paragraph below) and is promising for future low-cost large area flexible PSCs application.

VI. Dopant-free HTMs or controlled doping?

Most organic HTMs suffer from moderate intrinsic hole mobility so that doping is required to increase the conductivity of the hole transport layer. Doping, *i.e.* oxidation of the HTM, is usually achieved by adding 4-*tert*-butylpyridine (*t*BP) and lithium bis(trifluoromethanesulfonyl)imide (LiTFSI) additives to the precursor solution. Dopants, such as the typical cobalt (II) oxidant **FK209**, can also be used to further increase conductivity and photovoltaic performances. For instance, the PCE reportedly increases from 8.48% to 18.87% upon doping of the **SGT-405(3,6)** HTM layer in PSC, and from 8.13% to 17.71% using spiro-OMeTAD. [66] As mentioned above, the incorporation of additives induces stability issues related to morphological evolution of the HTM layer and creation of pinholes due to migration/evaporation of volatile additives (in particular free *t*BP) upon heating.[24,95] Also, LiTFSI is highly hygroscopic, which leads to accelerated performance drop in unencapsulated devices as the perovskite layer degrades faster.[96] The chemical reactivity of the nucleophilic *t*BP may be an additional issue. *t*BP has been identified as a cause of fast light-induced degradation of perovskite solar cells in the presence of gold, possibly due to the formation of pyridine:gold complexes.[97] Pyridination of spiro-OMeTAD as well as **V886** and **V990** HTMs was recently reported under thermal stress in doped HTM thin films.[98] Pyridination occurs at the 4 position of the carbazole moiety and is believed to proceed on the most electrophilic site of the oxidized species, in agreement with density functional theory (DFT) calculations of the lowest unoccupied molecular orbital (LUMO) of radical cation **V990^{+}** (Figure 2).[99] The pyridinated species exhibits lower HOMO and LUMO energy levels, which could create trap states for holes and alter electron-blocking properties. The power conversion efficiency of a PSC was indeed found to drop from 17.5 to 15.2% upon addition of 10 mol% **V886(tBP^{+})(TFSI^{-})** to a reference **V886** hole transport layer, thus pointing to a negative impact of tBP on PSC stability. The development of dopant-free HTMs on the one hand and precise doping control on the other are the two main emerging strategies that are currently being explored in order to achieve high efficiency while solving instability issues.

Dopant-free HTMs enabling high efficiency PSC without any additive or dopant are particularly appealing.[27] A few carbazole-based HTMs have been reported as efficient dopant-free HTMs so far. As detailed above, the **CMO** HTM led to 15.92% efficiency (close to the 16.70% recorded with doped spiro-OMeTAD), whereas substitution of the oxygen atoms with sulfur in the **CMT** molecule afforded a lower 12.91% PCE.[86,93] The dendrimer-like HTMs **3,6-BCz-OMeTAD** and **2,7-BCz-OMeTAD** exhibited 17.0 and 17.6% PCE, respectively, compared with 18.5% with

spiro-OMeTAD. Interestingly, a relatively high PCE of 16.09% was reported for **PVCz-OMeDAD**, showing that DMPA-substituted carbazoles can be advantageously incorporated in non-conjugated polymers. It is worth mentioning that this finding opens new perspectives given the ordinarily higher mechanical properties of polymer thin films, that could end up being required to improve the robustness of perovskite photovoltaic devices.[100] The lower solubility of polymers may also be valuable to fabricate inverted p-i-n PSC.

The reported achievements demonstrate that dopant-free HTMs are promising and deserve further investigation. They could help to improve the lifetime of perovskite solar cells. It can be noted however that all carbazole-based HTMs described here fail to afford power conversion efficiencies as high as those obtained with doped spiro-OMeTAD. This is consistent with the general trend observed with other dopant-free HTMs of any kind reported in the literature. Furthermore, dopant-free HTM layers are usually very thin. For instance, the HTM layer thickness of the best-performing devices incorporating **PVCz-OMeDAD**, **3,6-BCzOMeTAD** and **2,7-BCzOMeTAD** was 30 nm. It seems that the loss in conductivity compared with doped materials can only be compensated by reduced layer thickness. In turn, this may be a significant drawback when it comes to reproducibility and scalability as it is likely to increase the occurrence of shunts in large area solar cells. It seems desirable to look forward to increasing hole mobility of HTMs in order to fabricate high-performing photovoltaic devices with a slightly thicker dopant-free hole transport layer.

The second promising research direction involves dopant engineering and doping level control. The main interest of this strategy is the perspective of optimizing power conversion efficiency and pushing it beyond the efficiency of state-of-the-art spiro-OMeTAD-based devices while improving the stability at the same time. The doping mechanism has been investigated in the case of spiro-OMeTAD. In the absence of dopant, oxidation occurs only in the presence of oxygen since lithium is a very weak oxidant.[101] There are multiple related parameters that will likely affect device performances, such as the concentration of additives, tBP:LiTFSI ratio, chemical nature and concentration of dopant (if any), exposure to air (oxygen) and duration of solution stirring before film deposition. Furthermore, optimum HTM layer thickness will be a function of conductivity, which can be expected to vary not only from one HTM to another, but also with the doping level for a single HTM. The doping level itself was shown to depend strongly on the chemical dopant

properties.[102] Thus, optimization of the doping process is not straightforward. This implies that most HTM-containing perovskite solar cells reported in the literature can be considered as likely non-optimized. A recent study suggests that even the widely studied spiro-OMeTAD system with LiTFSI and tBP is not optimized.[96] Indeed, a 4:1 tBP:LiTFSI molar ratio was shown to bring both efficiency and stability enhancement over the conventional 6:1 mixture used in most studies. The results were attributed to the formation of a favorable tBP:LiTFSI complex without uncomplexed tBP left. In a separate work comparing three different copper-based dopants, Cheng *et al.* have demonstrated the influence of the redox potential of the dopant on doping efficiency and conductivity, but also on the interfacial recombination process at the perovskite/HTM interface.[102] The selection of the appropriate dopant followed by doping level tuning led to a significant increase of the power conversion efficiency from 13.0 to 19.3%. If spiro-OMeTAD hole transport layer can still be optimized after years of development, it seems reasonable to believe that the doping process of most newly reported HTMs could also be further improved.

Interestingly, Berry, Luther and co-workers have reported a new method for precisely controlling the doping level in a study where the HTM was the *N*-(2-ethylhexyl) carbazole-based **EH44** (previously published under the name **CMO**).[87] In this purpose, the oxidized **EH44-ox** radical cation (Figure 3) was isolated and mixed with **EH44** in order to make lithium-free hole transport layers with a controlled level of oxidized species. The optimal content of **EH44-ox** was found to be *ca.* 14 wt%. As indicated in Table 4, the champion cell reached a PCE of 18.5% (compared with 19.6% with spiro-OMeTAD). Most importantly, PSCs containing **EH44** tested under ISOS-L-1 conditions were much more stable than the reference cells fabricated with doped spiro-OMeTAD (Figure 3). The initial burn-in decay observed for FTO/TiO_2/$FA_xMA_yCs_{1-x-y}Pb(I_{1-x}Br_z)_3$/HTM/Au devices seems to be mainly related to the TiO_2/perovskite interface. Upon substitution of SnO_2 to TiO_2 and MoO_x/Al to Au, the devices were highly stable over 1,000 hours (retaining 94% of peak efficiency under identical conditions). However, although **CMO/EH44** was initially reported as an efficient dopant-free HTM in PSC, tBP was still found necessary to optimize device efficiency in this study, and its presence may be detrimental at a higher temperature. Indeed, a 40% performance drop was recorded after 100 hours under ISOS-L-2 testing conditions at high temperature (70°C) and relative humidity (50%). Thorough investigation of the role played by tBP (both at perovskite/HTM, HTM/metal interfaces and in the bulk of the HTM layer) would help designing strategies to either remove, neutralize or substitute it in PSC.

VII. Conclusions

The PCE of perovskite solar cells has dramatically increased since the first report of a stable solution-processed PSC in 2012, and is now competing with the commercial silicon, CdTe and CIGS photovoltaic technologies. Cost and stability issues, which can only partially be overcome by perovskite compositional tuning, are now the main limitations preventing the development of the perovskite technology. Since a hole transport layer is required to build efficient PSC devices, many research efforts have been devoted to the design and synthesis of new HTMs to replace the standard but expensive spiro-OMeTAD, most of them being nitrogen-rich organic materials. Organic HTMs present several advantages as they are compatible with low-temperature solution processing, and molecular engineering enables fine tuning of opto-electronic and thermal properties of the HTMs.

The potential of DMPA-containing carbazole derivatives as HTMs was first demonstrated by early works in DSSC, then in PSC. A large number of studies have now been published, accounting for several dozens of molecules. This review provides an overview of the different classes of DMPA-containing carbazole-based HTMs and highlights the synthetic pathways, the structure-property relationship and the advances obtained in PSC devices.

In most cases, given the various device architecture and perovskite compositions used from one study to another, photovoltaic parameters cannot be directly compared. Nonetheless, several of the recently reported carbazole-based HTMs appear to be very promising, with PCE close to or even exceeding the PCE of reference devices built with spiro-OMeTAD. The highest efficiencies are close to 19% PCE in mixed cation and/or mixed halide perovskite devices. Data stability, when reported, often indicate equivalent or enhanced lifetime. This is particularly true in the case of the few dopant-free carbazole-based HTMs, or when the doping level is precisely controlled in a lithium-free HTM layer.

Most of the synthesized carbazole-based HTMs are functionalized with DMPA in positions 3 and 6, where the functionalization is straightforward. Overall, the 2,7-substituted HTMs tend to slightly outperform the 3,6 homologues, but the reduced number of studies does not allow firm conclusions so far. The more complex synthesis of the 2,7 analogues makes them almost twice as expensive. On the other hand, they exhibit slightly shifted energy levels and higher glass transition

temperature. Whether potential performance or stability gains could be worth the higher cost remains to be seen.

The dendrimer-like HTMs (either twin or multi-arms star-shaped molecules) have afforded the best performances so far. It is obvious that a fully conjugated core linker is not necessary to reach high efficiencies. The CzDMPA units, on which the HOMO energy level is usually localized, are thought to be responsible for hole transport. Thus, it can be deduced that a sufficient content of CzDMPA is required. The ability to stack in a favourable way could be critical in order to promote intramolecular charge transport. Donor-acceptor type HTMs have demonstrated promising efficiencies. The electronic effect of the electron-accepting units is obvious, but the extended π-conjugated core structure could also enhance π-stacking and contribute to charge transport. At this point, the design of the HTMs remains largely empirical. Correlated computational and experimental investigations of intermolecular stacking and its influence on hole mobility would most likely provide valuable guidelines for the design of future HTMs.

Further structural variations recently introduced by synthetic chemists around the CzDMPA group include tetra-substitution of the carbazole at 1,3,6,8 positions in order to increase the number of methoxy functions and steric hindrance, replacement of the oxygen atoms in the DMPA units with the less electronegative sulfur atoms to tune energy levels and perovskite/HTM interactions, and introduction of an additional phenyl ring as π-linker between the carbazole and the DMPA. There are undoubtedly still numerous options to explore and molecular engineering of the HTMs will certainly offer solutions to improve charge extraction, charge transport and device stability. Furthermore, recent works highlight that achieving efficient dopant-free behaviour or highly controlled doping of the HTM layer holds great promise.

Acknowledgements

The authors would like to thank Ali Tarhini and Sandra El Rif for drawing the graphical abstract. They are also grateful to the CELEZ project supported by the Région Centre-Val-de-Loire, France, for its financial support.

References

[1] David B. Mitzi, Synthesis, Structure, and Properties of Organic-Inorganic Perovskites and Related Materials, Prog. Inorg. Chem. 48 (2007). doi:10.1002/9780470166499.ch1.

[2] A. Kojima, K. Teshima, Y. Shirai, T. Miyasaka, Organometal halide perovskites as visible-light sensitizers for photovoltaic cells, J. Am. Chem. Soc. 131 (2009) 6050–6051. doi:10.1021/ja809598r.

[3] H.S. Kim, C.R. Lee, J.H. Im, K.B. Lee, T. Moehl, A. Marchioro, S.J. Moon, R. Humphry-Baker, J.H. Yum, J.E. Moser, M. Grätzel, N.G. Park, Lead iodide perovskite sensitized all-solid-state submicron thin film mesoscopic solar cell with efficiency exceeding 9%, Sci. Rep. 2 (2012) 591. doi:10.1038/srep00591.

[4] M.M. Lee, J. Teuscher, T. Miyasaka, T.N. Murakami, H.J. Snaith, Efficient Hybrid Solar Cells Based on Meso-Superstructured Organometal Halide Perovskites, Science. 338 (2012) 643–648. doi:10.1126/science.1228604 [doi].

[5] W.S. Yang, B.-W. Park, E.H. Jung, N.J. Jeon, Iodide management in formamidinium-lead-halide – based perovskite layers for efficient solar cells, Science. 356 (2017) 1376–1379. doi:10.1126/science.aan2301.

[6] N.J. Jeon, H. Na, E.H. Jung, T.Y. Yang, Y.G. Lee, G. Kim, H.W. Shin, S. Il Seok, J. Lee, J. Seo, A fluorene-terminated hole-transporting material for highly efficient and stable perovskite solar cells, Nat. Energy. 3 (2018) 682–689. doi:10.1038/s41560-018-0200-6.

[7] National Renewable Energy Laboratory (NREL), Efficiency Chart, 2018.

[8] J.-W. Lee, D.-H. Kim, H.-S. Kim, S.-W. Seo, S.M. Cho, N.-G. Park, Formamidinium and Cesium Hybridization for Photo- and Moisture-Stable Perovskite Solar Cell, Adv. Energy Mater. 5 (2015) 1501310. doi:10.1002/aenm.201501310.

[9] C. Yi, J. Luo, S. Meloni, A. Boziki, N. Ashari-Astani, C. Grätzel, S.M. Zakeeruddin, U. Rothlisberger, G. Michael, Entropic stabilization of mixed A-cation ABX3 metal halide perovskites for high performance perovskite solar cells, Energy Environ. Sci. 9 (2016) 656–662. doi:10.1039/C5EE03255E.

[10] D. Son, S. Kim, J. Seo, H. Shin, D. Lee, N. Park, Universal Approach toward Hysteresis-Free Perovskite Solar Cell via Defect Engineering, J. Am. Chem. Soc. 140 (2018) 1358–1364. doi:10.1021/jacs.7b10430.

[11] L. Chen, Y. Tan, Z. Chen, T. Wang, S. Hu, Z. Nan, L. Xie, Y. Hui, L. Xie, Y. Hui, J. Huang, C. Zhan, S. Wang, J.-Z. Zhou, J.-W. Yan, B.-W. Mao, Z. Tian, Toward long-term stability : single crystal alloys of cesium- containing mixed cations and mixed halides perovskite, J. Am. Chem. Soc. (2019) doi: 10.1021/jacs.8b11610.

[12] H. Kim, A. Hagfeldt, N. Park, Morphological and compositional progress in halide perovskite solar cells, Chem. Commun. (2019) doi: 10.1039/c8cc08653b.

[13] K.T. Cho, S. Orlandi, M. Cavazzini, I. Zimmermann, A. Lesch, N. Tabet, G. Pozzi, G. Grancini, M.K. Nazeeruddin, A water-repellent low dimensional fluorous perovskite as

interfacial coating for 20 % efficient solar cells, Nano Lett. 18 (2018) 5467–5474. doi:10.1021/acs.nanolett.8b01863.

[14] F.J. Ramosa, T. Maindron, S. Béchua, A. Rebai, M. Frégnaux, M. Bouttemya, J. Rousseta, P. Schulza, N. Schneider, Versatile Perovskite Solar Cell Encapsulation by Low-Temperature ALD-Al2O3 with Long-Term Stability Improvement, Sustain. Energy Fuels. 2 (2018) 2468–2479. doi:10.1039/C8SE00282G.

[15] A. Cho, N. Park, Impact of Interfacial Layers in Perovskite Solar Cells, ChemSusChem. 10 (2017) 3687–3704. doi:10.1002/cssc.201701095.

[16] Q. Wang, N. Phung, D. Girolamo, P. Vivo, A. Abate, Environmental Science Enhancement in lifespan of halide perovskite solar cells, Energy Environ. Sci. (2018) doi : 10.1039/c8ee02852d.

[17] H. Zhou, Q. Chen, G. Li, S. Luo, T. Song, H.-S. Duan, Z. Hong, J. You, Y. Liu, Y. Yang, Interface engineering of highly efficient perovskite solar cells, Science. 345 (2014) 542–546. doi:10.1126/science.1254050.

[18] J.W. Lee, Z. Dai, C. Lee, H.M. Lee, T.H. Han, N. De Marco, O. Lin, C.S. Choi, B. Dunn, J. Koh, D. Di Carlo, J.H. Ko, H.D. Maynard, Y. Yang, Tuning Molecular Interactions for Highly Reproducible and Efficient Formamidinium Perovskite Solar Cells via Adduct Approach, J. Am. Chem. Soc. 140 (2018) 6317–6324. doi:10.1021/jacs.8b01037.

[19] M. Saliba, T. Matsui, K. Domanski, J.-Y. Seo, A. Ummadisingu, S.M. Zakeeruddin, W.R.T. Juan-Pablo Correa-Baena, A. Abate, A. Hagfeldt, M. Grätzel, Incorporation of rubidium cations into perovskite solar cells improves photovoltaic performance, Science. 354 (2016) 206–209. doi:10.1126/science.aah5557.

[20] H. Tan, A. Jain, O. Voznyy, X. Lan, F.P.G. De Arquer, J.Z. Fan, R. Quintero-Bermudez, M. Yuan, B. Zhang, Y. Zhao, F. Fan, P. Li, L.N. Quan, Y. Zhao, Z.H. Lu, Z. Yang, S. Hoogland, E.H. Sargent, Efficient and stable solution-processed planar perovskite solar cells via contact passivation, Science. 355 (2017) 722–726. doi:10.1126/science.aai9081.

[21] A. Krishna, A.C. Grimsdale, Hole transporting materials for mesoscopic perovskite solar cells – towards a rational design, J. Mater. Chem. A. 5 (2017) 16446–16466. doi:10.1039/C7TA01258F.

[22] T. Malinauskas, D. Tomkute-Luksiene, R. Sens, M. Daskeviciene, R. Send, H. Wonneberger, V. Jankauskas, I. Bruder, V. Getautis, Enhancing thermal stability and lifetime of solid-state dye-sensitized solar cells via molecular engineering of the hole-transporting material spiro-OMeTAD, ACS Appl. Mater. Interfaces. 7 (2015) 11107–11116. doi:10.1021/am5090385.

[23] X. Zhao, H.-S. Kim, J.-Y. Seo, N.-G. Park, Effect of Selective Contacts on Thermal Stability of Perovskite Solar Cell, ACS Appl. Mater. Interfaces. 9 (2017) 7148–7153. doi:10.1021/acsami.6b15673.

[24] S. Wang, M. Sina, P. Parikh, T. Uekert, B. Shahbazian, A. Devaraj, Y.S. Meng, Role of 4-tert-Butylpyridine as a Hole Transport Layer Morphological Controller in Perovskite Solar Cells, Nano Lett. 16 (2016) 5594–5600. doi:10.1021/acs.nanolett.6b02158.

[25] N. Arora, M.I. Dar, A. Hinderhofer, N. Pellet, F. Schreiber, S.M. Zakeeruddin, M. Grätzel, Perovskite solar cells with CuSCN hole extraction layers yield stabilized efficiencies greater than 20%, Science. 358 (2017) 768–771. doi:10.1126/science.aam5655.

[26] J. Urieta-Mora, I. García-Benito, A. Molina-Ontoria, N. Martín, Hole transporting materials for perovskite solar cells: a chemical approach, Chem. Soc. Rev. 47 (2018) 8541–8571. doi:10.1039/C8CS00262B.

[27] W. Zhou, Z. Wen, P. Gao, Less is More: Dopant-Free Hole Transporting Materials for High-Efficiency Perovskite Solar Cells, Adv. Energy Mater. 8 (2018) 1702512. doi:10.1002/aenm.201702512.

[28] E. Rezaee, X. Liu, Q. Hu, L. Dong, Q. Chen, J. Pan, Dopant-Free Hole Transporting Materials for Perovskite Solar Cells, Sol. RRL. 1800200 (2018) 1–38. doi:10.1002/solr.201800200.

[29] S.J. Park, S. Jeon, I.K. Lee, J. Zhang, H. Jeong, J.Y. Park, J. Bang, T.K. Ahn, H.W. Shin, B.G. Kim, H.J. Park, Inverse Type Planar Heterojunction Perovskite Solar Cells with Dopant Free Hole Transporting Material: Lewis Base-Assisted Passivation and Charge Recombination, J. Mater. Chem. A. 5 (2017) 13220–13227. doi:10.1039/c7ta02440a.

[30] F. Cai, J. Cai, L. Yang, W. Li, R.S. Gurney, H. Yi, A. Iraqi, D. Liu, T. Wang, Molecular engineering of conjugated polymers for efficient hole transport and defect passivation in perovskite solar cells, Nano Energy. 45 (2018) 28–36. doi:10.1016/j.nanoen.2017.12.028.

[31] M. Saliba, S. Orlandi, T. Matsui, S. Aghazada, M. Cavazzini, J.-P. Correa-Baena, P. Gao, R. Scopelliti, E. Mosconi, K.-H. Dahmen, F. De Angelis, A. Abate, A. Hagfeldt, G. Pozzi, M. Grätzel, M.K. Nazeeruddin, A molecularly engineered hole-transporting material for efficient perovskite solar cells, Nat. Energy. 1 (2016) 15017–15023. doi:10.1038/nenergy.2015.17.

[32] B. Xu, D. Bi, Y. Hua, P. Liu, M. Cheng, M. Grätzel, L. Kloo, A. Hagfeldt, L. Sun, A low-cost spiro[fluorene-9,9′-xanthene]-based hole transport material for highly efficient solid-state dye-sensitized solar cells and perovskite solar cells, Energy Environ. Sci. 9 (2016) 873–877. doi:10.1039/C6EE00056H.

[33] F. Zhang, X. Liu, C. Yi, D. Bi, J. Luo, S. Wang, X. Li, Y. Xiao, S.M. Zakeeruddin, M. Grätzel, Dopant-Free Donor (D)–π–D–π–D Conjugated Hole-Transport Materials for Efficient and Stable Perovskite Solar Cells, ChemSusChem. 9 (2016) 2578–2585. doi:10.1002/cssc.201600905.

[34] P. Agarwala, D. Kabra, A review on triphenylamine (TPA) based organic hole transport materials (HTMs) for dye sensitized solar cells (DSSCs) and perovskite solar cells (PSCs): evolution and molecular engineering, J. Mater. Chem. A. 5 (2017) 1348–1373. doi:10.1039/C6TA08449D.

[35] K. Rakstys, A. Abate, M.I. Dar, P. Gao, V. Jankauskas, G. Jacopin, E. Kamarauskas, S. Kazim, S. Ahmad, M. Grätzel, M.K. Nazeeruddin, Triazatruxene-Based Hole Transporting Materials for Highly Efficient Perovskite Solar Cells, J. Am. Chem. Soc. 137 (2015) 16172–16178. doi:10.1021/jacs.5b11076.

[36] C. Huang, W. Fu, C.-Z. Li, Z. Zhang, W. Qiu, M. Shi, P. Heremans, A.K.-Y. Jen, H. Chen, Dopant-Free Hole-Transporting Material with a C 3 h Symmetrical Truxene Core for Highly Efficient Perovskite Solar Cells, J. Am. Chem. Soc. 138 (2016) 2528–2531. doi:10.1021/jacs.6b00039.

[37] I. García-Benito, I. Zimmermann, J. Urieta-Mora, J. Aragó, A. Molina-Ontoria, E. Ortí, N. Martín, M.K. Nazeeruddin, Isomerism effect on the photovoltaic properties of benzotrithiophene-based hole-transporting materials, J. Mater. Chem. A. 5 (2017) 8317–8324. doi:10.1039/c7ta00997f.

[38] T. Leijtens, I.K. Ding, T. Giovenzana, J.T. Bloking, M.D. McGehee, A. Sellinger, Hole transport materials with low glass transition temperatures and high solubility for application in solid-state dye-sensitized solar cells, ACS Nano. 6 (2012) 1455–1462. doi:10.1021/nn204296b.

[39] G. Puckyte, B. Schmaltz, A. Tomkeviciene, M. Degbia, J. V. Grazulevicius, H. Melhem, J. Bouclé, F. Tran-Van, Carbazole-based molecular glasses for efficient solid-state dye-sensitized solar cells, J. Power Sources. 233 (2013) 86–92. doi:10.1016/j.jpowsour.2013.01.137.

[40] M. Degbia, B. Schmaltz, J. Bouclé, J. V. Grazulevicius, F. Tran-Van, Carbazole based hole transporting materials for solid state dye sensitizer solar cells: Role of the methoxy groups, Polym. Int. 63 (2014) 1387–1393. doi:10.1002/pi.4727.

[41] B. Xu, E. Sheibani, P. Liu, J. Zhang, H. Tian, N. Vlachopoulos, G. Boschloo, L. Kloo, A. Hagfeldt, L. Sun, Carbazole-Based Hole-Transport Materials for Efficient Solid-State Dye-Sensitized Solar Cells and Perovskite Solar Cells, Adv. Mater. 26 (2014) 6629–6634. doi:10.1002/adma.201402415.

[42] A. Tomkeviciene, G. Puckyte, J. Vidas, M. Degbia, F. Tran-Van, B. Schmaltz, V. Jankauskas, J. Bouclé, Diphenylamino-substituted derivatives of 9-phenylcarbazole as glass-forming hole-transporting materials for solid state dye sensitized solar cells, Synth. Met. 162 (2012) 1997–2004. doi:10.1016/j.synthmet.2012.10.002.

[43] S. Benhattab, R. Nakar, J.W.R. Acosta, N. Berton, F. Tran-Van, B. Schmaltz, Carbazole-based twin molecules as hole-transporting materials in dye-sensitized solar cells, Dye. Pigment. 151 (2018) 238–244. doi:10.1016/j.dyepig.2017.12.050.

[44] A. Magomedov, S. Paek, P. Gratia, E. Kasparavicius, M. Daskeviciene, E. Kamarauskas, A. Gruodis, V. Jankauskas, K. Kantminiene, K.T. Cho, K. Rakstys, T. Malinauskas, V. Getautis, M.K. Nazeeruddin, Diphenylamine-Substituted Carbazole-Based Hole Transporting Materials for Perovskite Solar Cells: Influence of Isomeric Derivatives, Adv. Funct. Mater. 28 (2018) 1704351. doi:10.1002/adfm.201704351.

[45] Š. Daškevičiū tė, N. Sakai, M. Franckevičius, M. Daškevičienė, A. Magomedov, V. Jankauskas, H.J. Snaith, V. Getautis, Nonspiro, Fluorene-Based, Amorphous Hole Transporting Materials for Efficient and Stable Perovskite Solar Cells, Adv. Sci. 5 (2018) 1700811. doi:10.1002/advs.201700811.

[46] Donald A.Tomalia, H. Baker, J. Dewald, M.Hall., G.Kallos, S. Martin, J. Raeck, J. Ryder, P. Smith, Dendritic Macromolecules: Synthesis of Starburst Dendrimers, Macromolecules.

19 (1986) 2466–2468. doi:10.1021/ma00163a029.

[47] C.J. Hawker, J.M.J. Fréchet, Preparation of Polymers with Controlled Molecular Architecture. A New Convergent Approach to Dendritic Macromolecules, J. Am. Chem. Soc. 112 (1990) 7638–7647. doi:10.1021/ja00177a027.

[48] M. Degbia, B. Schmaltz, F. Tran-Van, Nouveaux synthons pour l'elaboration de semi-conducteurs organiques, (2016) WO2016016221.

[49] https://www.ikambaorganics.com.

[50] L. Zhu, Y. Shan, R. Wang, D. Liu, C. Zhong, Q. Song, High-Efficiency Perovskite Solar Cells Based on New TPE Compounds as Hole Transport Materials : The Role of 2,7- and 3,6-Substituted Carbazole Derivatives, Chem. - A Eur. J. 23 (2017) 4373–4379. doi:10.1002/chem.201605187.

[51] M.S. Kang, S. Do Sung, I.T. Choi, H. Kim, M. Hong, J. Kim, W.I. Lee, H.K. Kim, Novel Carbazole-Based Hole-Transporting Materials with Star-Shaped Chemical Structures for Perovskite-Sensitized Solar Cells, ACS Appl. Mater. Interfaces. 7 (2015) 22213–22217. doi:10.1021/acsami.5b04662.

[52] S. Do Sung, M.S. Kang, I.T. Choi, H.M. Kim, H. Kim, M. Hong, H.K. Kim, W.I. Lee, 14.8% Perovskite Solar Cells Employing Carbazole Derivatives As Hole Transporting Materials, Chem. Commun. 50 (2014) 14161–14163. doi:10.1039/C4CC06716A.

[53] S. Benhattab, A.N. Cho, R. Nakar, N. Berton, F. Tran-Van, N.G. Park, B. Schmaltz, Simply designed carbazole-based hole transporting materials for efficient perovskite solar cells, Org. Electron. 56 (2018) 27–30. doi:10.1016/j.orgel.2017.12.031.

[54] F. Wu, Y. Ji, C. Zhong, Y. Liu, L. Tan, L. Zhu, Fluorine-substituted benzothiadiazole-based hole transport materials for highly efficient planar perovskite solar cells with a FF exceeding 80%, Chem. Commun. 53 (2017) 8719–8722. doi:10.1039/c7cc04606e.

[55] M. Li, Z. Wang, M. Liang, L. Liu, X. Wang, Z. Sun, S. Xue, Low-Cost Carbazole-Based Hole-Transporting Materials for Perovskite Solar Cells: Influence of S,N-Heterocycle, J. Phys. Chem. C. 122 (2018) 24014–24024. doi:10.1021/acs.jpcc.8b09482.

[56] C. Yin, J. Lu, Y. Xu, Y. Yun, K. Wang, J. Li, L. Jiang, J. Sun, A.D. Scully, F. Huang, J. Zhong, J. Wang, Y. Cheng, T. Qin, W. Huang, Low-Cost N,N′-Bicarbazole-Based Dopant-Free Hole- Transporting Materials for Large-Area Perovskite Solar Cells, Adv. Energy Mater. 8 (2018) 1800538. doi:10.1002/aenm.201800538.

[57] U. Bach, D. Lupo, P. Comte, J.E. Moser, F. Weissörtel, J. Salbeck, H. Spreitzer, M. Grätzel, Solid-state dye-sensitized mesoporous TiO2 solar cells with high photon-to-electron conversion efficiencies, Nature. 395 (1998) 583–585. doi:10.1038/26936.

[58] T.T. Bui, F. Goubard, J. Troughton, T. Watson, Simple 3,6-bis(diphenylaminyl)carbazole molecular glasses as hole transporting materials for hybrid perovskite solar cells, J. Mater. Sci. Mater. Electron. 28 (2017) 17551–17556. doi:10.1007/s10854-017-7691-y.

[59] T.T. Bui, S.K. Shah, M. Abbas, X. Sallenave, G. Sini, L. Hirsch, F. Goubard, Carbazole-Based Molecular Glasses as Hole-Transporting Materials in Solid State Dye-Sensitized

Solar Cells, ChemNanoMat. 1 (2015) 203–210. doi:10.1002/cnma.201500014.

[60] M. Degbia, Semi-conducteurs organiques π-conjugués pour l'élaboration de dispositifs photovoltaïques hybrides solides à colorant. PHD thesis. Université de Tours, 2014.

[61] W. Qiao, Y. Chen, F. Li, X. Zong, Z. Sun, M. Liang, S. Xue, Novel efficient hole-transporting materials based on a 1,1′-bi-2-naphthol core for perovskite solar cells, RSC Adv. 7 (2017) 482–492. doi:10.1039/c6ra25606f.

[62] J. Wang, Y. Chen, F. Li, X. Zong, J. Guo, Z. Sun, S. Xue, A new carbazole-based hole-transporting material with low dopant content for perovskite solar cells, Electrochim. Acta. 210 (2016) 673–680. doi:10.1016/j.electacta.2016.05.203.

[63] X. Zong, W. Qiao, Y. Chen, Z. Sun, M. Liang, S. Xue, A new binaphthol based hole-transporting materials for perovskite solar cells, Tetrahedron. 73 (2017) 3398–3405. doi:10.1016/j.tet.2017.05.020.

[64] F. Wu, Y. Ji, R. Wang, Y. Shan, L. Zhu, Molecular engineering to enhance perovskite solar cell performance: Incorporation of benzothiadiazole as core unit for low cost hole transport materials, Dye. Pigm. 143 (2017) 356–360. doi:10.1016/j.dyepig.2017.04.059.

[65] A. Molina-ontoria, I. Zimmermann, I. Garcia-benito, P. Gratia, C. Roldµn-carmona, S. Aghazada, M. Grätzel, M.K. Nazeeruddin, N. Martín, Benzotrithiophene-Based Hole-Transporting Materials for 18.2% Perovskite Solar Cells, Angew. Chemie. 128 (2016) 6378–6382. doi:10.1002/ange.201511877.

[66] C. Lu, I.T. Choi, J. Kim, H.K. Kim, Simple synthesis and molecular engineering of low-cost and star-shaped carbazole-based hole transporting materials for highly efficient perovskite solar cells, J. Mater. Chem. A. 5 (2017) 20263–20276. doi:10.1039/c7ta04762b.

[67] R. Nakar, A.-N. Cho, N. Berton, J. Faure-Vincent, F. Tran-Van, N.-G. Park, B. Schmaltz, Triphenylamine 3 , 6 - carbazole derivative as hole - transporting material for mixed cation perovskite solar cells, Chem. Pap. 72 (2018) 1779–1787. doi:10.1007/s11696-018-0484-9.

[68] V. Jankauskas, H.J. Snaith, V. Getautis, M. Franckevic, Amorphous Hole-Transporting Material based on 2 , 2 ' -Bis- substituted 1 , 1 ' -Biphenyl Scaffold for Application in Perovskite Solar Cells, Chem. Asian J. 12 (2017) 958–962. doi:10.1002/asia.201700173.

[69] F. Wu, Y. Shan, J. Qiao, C. Zhong, R. Wang, Q. Song, L. Zhu, Replacement of Biphenyl by Bipyridine Enabling Powerful Hole Transport Materials for Efficient Perovskite Solar Cells, ChemSusChem. 10 (2017) 3833–3838. doi:10.1002/cssc.201700973.

[70] P. Gratia, A. Magomedov, T. Malinauskas, M. Daskeviciene, A. Abate, S. Ahmad, M. Grätzel, V. Getautis, M.K. Nazeeruddin, A Methoxydiphenylamine-Substituted Carbazole Twin Derivative: An Efficient Hole-Transporting Material for Perovskite Solar Cells, Angew. Chemie Int. Ed. 54 (2015) 11409–11413. doi:10.1002/anie.201504666.

[71] V. Mimaite, J.V. Grazulevicius, R. Laurinaviciute, D. Volyniuk, V. Jankauskas, G. Sini, Can Hydrogen Bonds Improve the Hole-Mobility in Amorphous Organic Semiconductors? Experimental and Theoretical Insights, J. Mater.Chem C. 3 (2015) 11660. doi:10.1039/C5TC02534F.

[72] T. Malinauskas, D. Tomkute-Luksiene, R. Sens, M. Daskeviciene, R. Send, H. Wonneberger, V. Jankauskas, I. Bruder, V. Getautis, Enhancing thermal stability and lifetime of solid-state dye-sensitized solar cells via molecular engineering of the hole-transporting material spiro-OMeTAD, ACS Appl. Mater. Interfaces. 7 (2015) 11107–11116. doi:10.1021/am5090385.

[73] T. Qin, W. Huang, J. Kim, D. Vak, C. Forsyth, C.R. Mcneill, Y. Cheng, Nano Energy Amorphous hole-transporting layer in slot-die coated perovskite solar cells, Nano Energy. 31 (2017) 210–217. doi:10.1016/j.nanoen.2016.11.022.

[74] T.T. Bui, F. Goubard, J. Troughton, T. Watson, Simple 3 , 6-bis (diphenylaminyl) carbazole molecular glasses as hole transporting materials for hybrid perovskite solar cells, J. Mater. Sci. Mater. Electron. 28 (2017) 17551–17556. doi:10.1007/s10854-017-7691-y.

[75] N.J. Jeon, H.G. Lee, Y.C. Kim, J. Seo, J.H. Noh, J. Lee, S. Il Seok, O-methoxy substituents in spiro-OMeTAD for efficient inorganic-organic hybrid perovskite solar cells, J. Am. Chem. Soc. 136 (2014) 7837–7840. doi:10.1021/ja502824c.

[76] T. Leijtens, T. Giovenzana, S.N. Habisreutinger, J.S. Tinkham, N.K. Noel, B.A. Kamino, G. Sadoughi, A. Sellinger, H.J. Snaith, Hydrophobic Organic Hole Transporters for Improved Moisture Resistance in Metal Halide Perovskite Solar Cells, ACS Appl. Mater. Interfaces. 8 (2016) 5981–5989. doi:10.1021/acsami.5b10093.

[77] W. Yu, S. Yu, J. Zhang, W. Lianga, X. Wang, X. Guo, C. Li, AState, Two-in-one additive-engineering strategy for improved air stability of planar perovskite solar cells, Nano Energy. 45 (2017) 229. doi:10.1016/j.nanoen.2017.12.041.

[78] M. Degbia, M. Ben Manaa, B. Schmaltz, N. Berton, J. Bouclé, R. Antony, F. Tran-Van, Carbazole-based hole transporting material for solid state dye-sensitized solar cells: Influence of the purification methods, Mater. Sci. Semicond. Process. 43 (2016) 90–95. doi:10.1016/j.mssp.2015.12.004.

[79] A. Magomedov, A. Al-Ashouri, E. Kasparavičius, S. Strazdaite, G. Niaura, M. Jošt, T. Malinauskas, S. Albrecht, V. Getautis, Self-Assembled Hole Transporting Monolayer for Highly Efficient Perovskite Solar Cells, Adv. Energy Mater. 8 (2018) 1801892. doi:10.1002/aenm.201801892.

[80] Y. Shi, K. Hou, Y. Wang, K. Wang, H. Ren, M. Pang, F. Chen, S. Zhang, Two methoxyaniline-substituted dibenzofuran derivatives as hole-transport materials for perovskite solar cells, J. Mater. Chem. A. 4 (2016) 5415–5422. doi:10.1039/c6ta00976j.

[81] D. Li, J.Y. Shao, Y. Li, Y. Li, L.Y. Deng, Y.W. Zhong, Q. Meng, New hole transporting materials for planar perovskite solar cells, Chem. Commun. 54 (2018) 1651–1654. doi:10.1039/c7cc08985f.

[82] X. Wang, J. Zhang, S. Yu, W. Yu, P. Fu, X. Liu, D. Tu, X. Guo, C. Li, Lowering Molecular Symmetry To Improve the Morphological Properties of the Hole-Transport Layer for Stable Perovskite Solar Cells, Angew. Chemie - Int. Ed. 57 (2018) 12529–12533. doi:10.1002/anie.201807402.

[83] J.R. Witker, D.; Reynolds, Soluble variable color carbazole-containing electrochromic

polymers., Macromolecules. 38 (2005) 7636–7644. doi:10.1021/ma050805x.

[84] N. Berton, C. Ottone, V. Labet, R. De Bettignies, S. Bailly, A. Grand, C. Morell, S. Sadki, F. Chandezon, New alternating copolymers of 3,6-carbazoles and dithienylbenzothiadiazoles: Synthesis, characterization, and application in photovoltaics, Macromol. Chem. Phys. 212 (2011) 2127–2141. doi:10.1002/macp.201100209.

[85] N. Blouin, A. Michaud, D. Gendron, S. Wakim, E. Blair, R. Neagu-Plesu, M. Belletête, G. Durocher, Y. Tao, M. Leclerc, Toward a rational design of poly(2,7-carbazole) derivatives for solar cells, J. Am. Chem. Soc. 130 (2008) 732–742. doi:10.1021/ja0771989.

[86] J. Zhang, L.J. Xu, P. Huang, Y. Zhou, Y.Y. Zhu, N.Y. Yuan, J.N. Ding, Z.G. Zhang, Y.F. Li, A simple and dopant-free hole-transporting material based on (2-ethylhexyl)-9H-carbazole for efficient planar perovskite solar cells, J. Mater. Chem. C. 5 (2017) 12752–12757. doi:10.1039/c7tc03683c.

[87] J.A. Christians, P. Schulz, J.S. Tinkham, T.H. Schloemer, S.P. Harvey, B.J. Tremolet De Villers, A. Sellinger, J.J. Berry, J.M. Luther, Tailored interfaces of unencapsulated perovskite solar cells for >1,000 hour operational stability, Nat. Energy. 3 (2018) 68–74. doi:10.1038/s41560-017-0067-y.

[88] Z. Chen, H. Li, X. Zheng, Q. Zhang, Z. Li, Y. Hao, Low-Cost Carbazole-Based Hole-Transport Material for Highly Efficient Perovskite Solar Cells, Chems. 10 (2017) 3111–3117. doi:10.1002/cssc.201700678.

[89] J. Zhang, B. Xu, M.B. Johansson, N. Vlachopoulos, G. Boschloo, L. Sun, Strategy to Boost the E ffi ciency of Mixed-Ion Perovskite Solar Cells: Changing Geometry of the Hole Transporting Material, ACS Nano. 10 (2016) 6816–6825. doi:10.1021/acsnano.6b02442.

[90] X. Liu, X. Shi, C. Liu, Y. Ren, Y. Wu, W. Yang, A Simple Carbazole-Triphenylamine Hole Transport Material for Perovskite Solar Cells, J. Phys. Chem. C. 122 (2018) 26337–26343. doi:10.1021/acs.jpcc.8b08168.

[91] X. Yin, L. Guan, J. Yu, D. Zhao, C. Wang, N. Shrestha, Y. Han, Q. An, J. Zhou, B. Zhou, Y. Yu, C.R. Grice, One-step facile synthesis of a simple carbazole-cored hole transport material for high-performance perovskite solar cells, Nano Energy. 40 (2017) 163–169. doi:10.1016/j.nanoen.2017.08.016.

[92] X. Yin, C. Wang, D. Zhao, N. Shrestha, C.R. Grice, L. Guan, Z. Song, C. Chen, C. Li, G. Chi, B. Zhou, J. Yu, Binary hole transport materials blending to linearly tune HOMO level for high efficiency and stable perovskite solar cells, Nano Energy. 51 (2018) 680–687. doi:10.1016/j.nanoen.2018.07.027.

[93] L. Xu, P. Huang, J. Zhang, X. Jia, Z. Ma, Y. Sun, Y. Zhou, N.-Y. Yuan, J.-N. Ding, N,N-Di-para-methylthiophenylamine-Substituted (2-Ethylhexyl)-9H-Carbazole: A Simple, Dopant-Free Hole-Transporting Material for Planar Perovskite Solar Cells, J. Phys. Chem. C. 121 (2017) 21821–21826. doi:10.1021/acs.jpcc.7b04469.

[94] Y. Xu, T. Bu, M. Li, T. Qin, C. Yin, N. Wang, R. Li, J. Zhong, F. Huang, H. Li, Y. Peng, J. Wang, L. Xie, W. Huang, Non-Conjugated Polymer as an Efficient Transporting Material for Perovskite Solar Cells, ChemSusChem. 10 (2017) 2578–2584.

doi:10.1002/cssc.201700584.

[95] Z. Hawash, L.K. Ono, S.R. Raga, M. V. Lee, Y. Qi, Air-exposure induced dopant redistribution and energy level shifts in spin-coated Spiro-Meotad films, Chem. Mater. 27 (2015) 562–569. doi:10.1021/cm504022q.

[96] S. Wang, Z. Huang, X. Wang, Y. Li, M. Günther, S. Valenzuela, P. Parikh, A. Cabreros, W. Xiong, Y.S. Meng, Unveiling the Role of tBP-LiTFSI Complexes in Perovskite Solar Cells, J. Am. Chem. Soc. 140 (2018) 16720–16730. doi:10.1021/jacs.8b09809.

[97] J.P. Bastos, U.W. Paetzold, R. Gehlhaar, W. Qiu, D. Cheyns, S. Surana, V. Spampinato, T. Aernouts, J. Poortmans, Light-Induced Degradation of Perovskite Solar Cells: The Influence of 4-Tert-Butyl Pyridine and Gold, Adv. Energy Mater. 8 (2018) 1800554. doi:10.1002/aenm.201800554.

[98] E. Kasparavicius, A. Magomedov, T. Malinauskas, V. Getautis, Long-Term Stability of the Oxidized Hole-Transporting Materials used in Perovskite Solar Cells, Chem. - A Eur. J. 24 (2018) 9910–9918. doi:10.1002/chem.201801441.

[99] A. Magomedov, E. Kasparavičius, K. Rakstys, S. Paek, N. Gasilova, K. Genevičius, G. Juška, T. Malinauskas, M.K. Nazeeruddin, V. Getautis, Pyridination of hole transporting material in perovskite solar cells questions the long-term stability, J. Mater. Chem. C. 6 (2018) 8874–8878. doi:10.1039/c8tc02242a.

[100] J. Yang, B.D. Siempelkamp, D. Liu, T.L. Kelly, Investigation of CH3NH3PbI3 degradation rates and mechanisms in controlled humidity environments using in situ techniques, ACS Nano. 9 (2015) 1955–1963. doi:10.1021/nn506864k.

[101] A. Abate, T. Leijtens, S. Pathak, J. Teuscher, R. Avolio, M.E. Errico, J. Kirkpatrik, J.M. Ball, P. Docampo, I. McPherson, H.J. Snaith, Lithium salts as “redox active” p-type dopants for organic semiconductors and their impact in solid-state dye-sensitized solar cells, Phys. Chem. Chem. Phys. 15 (2013) 2572–2579. doi:10.1039/C2CP44397J.

[102] J. Zhang, Q. Daniel, T. Zhang, X. Wen, B. Xu, L. Sun, U. Bach, Y.B. Cheng, Chemical Dopant Engineering in Hole Transport Layers for Efficient Perovskite Solar Cells: Insight into the Interfacial Recombination, ACS Nano. 12 (2018) 10452–10462. doi:10.1021/acsnano.8b06062.

DMPA-containing carbazole-based hole transporting materials for perovskite solar cells: recent advances and perspectives

Nicolas Berton, Rana Nakar, Bruno Schmaltz*

Laboratoire de Physico-Chimie des Matériaux et des Electrolytes pour l'Energie (PCM2E), Université de Tours, Parc de Grandmont, Tours 37200, France

* Corresponding author : bruno.schmaltz@univ-tours.fr

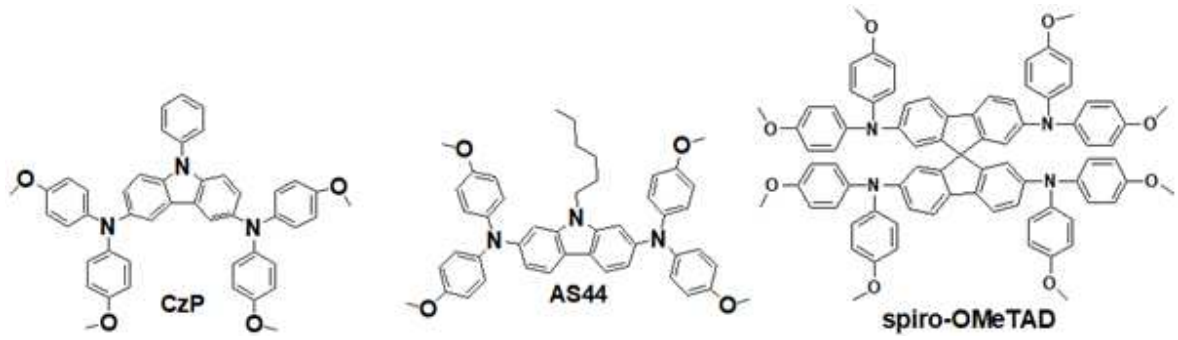

Scheme 1. Chemical structure of 3,6- (**CzP**), 2,7- (**AS44**) DMPA-substituted carbazole HTMs and spiro-OMeTAD.

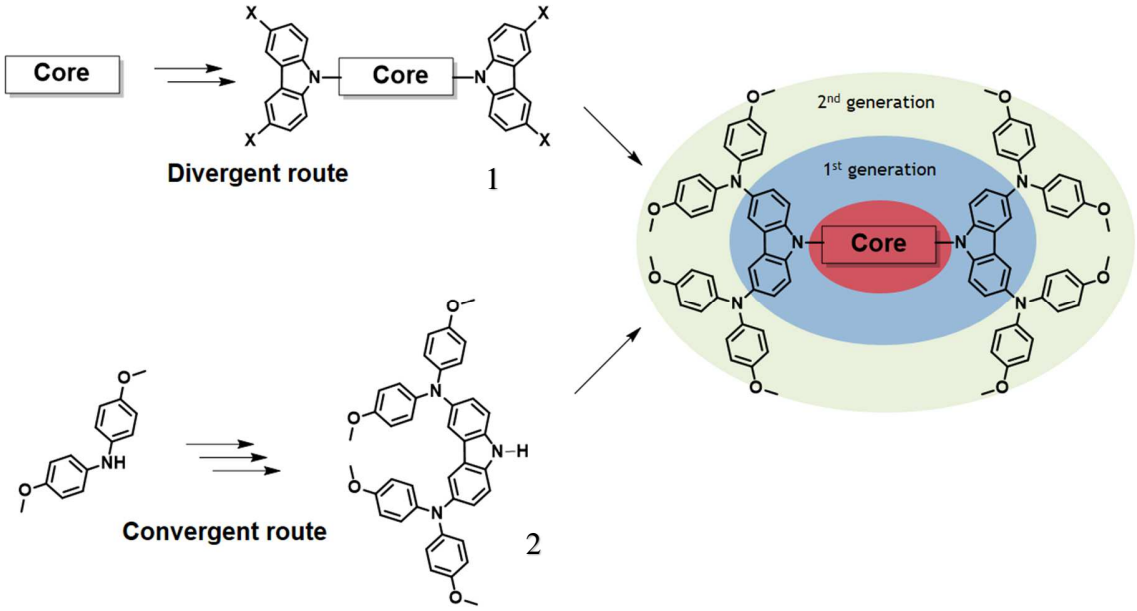

Scheme 2. Convergent and divergent synthetic pathways to obtain the 3,6-carbazole based pseudo-dendrimer.

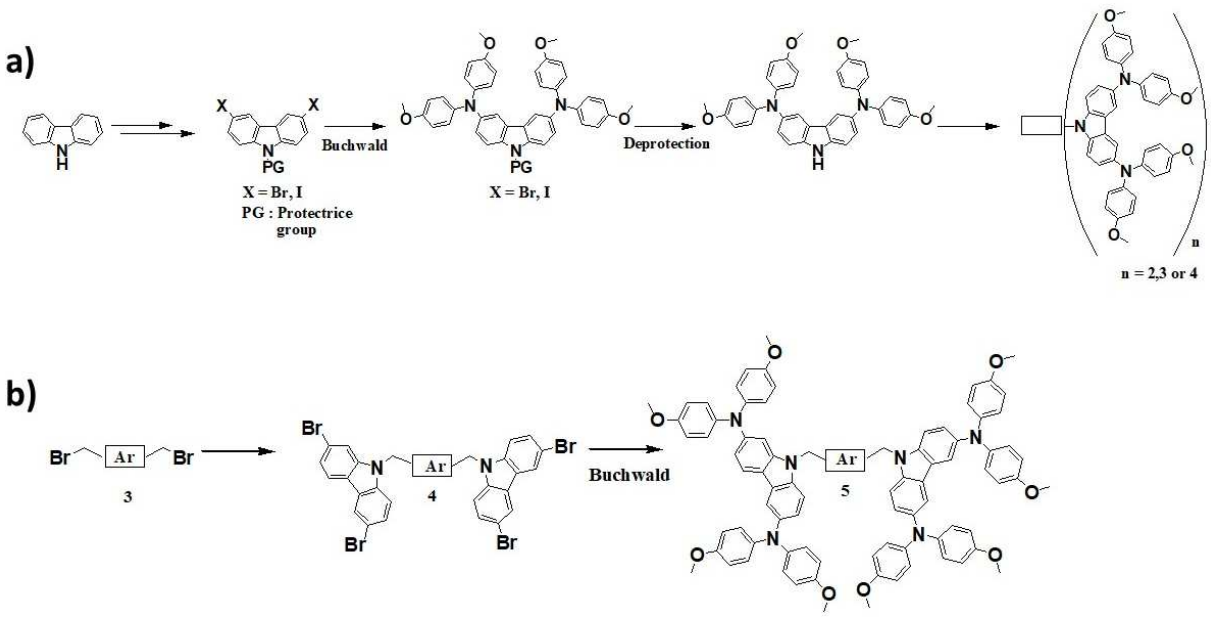

Scheme 3. Synthetic route to obtain CzDMPA-based HTMs HTMs via a) a convergent and b) divergent strategy.

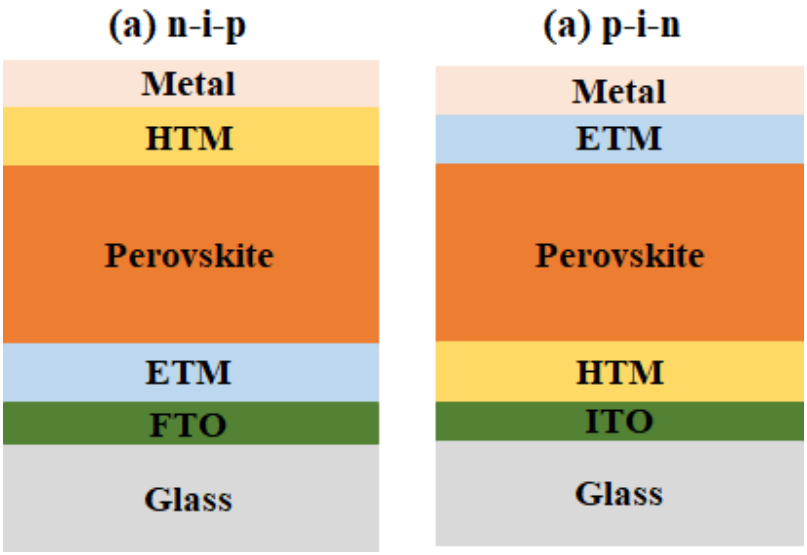

Figure 1. Architecture of a (a) conventional n-i-p and (b) inverse p-i-n PSC.

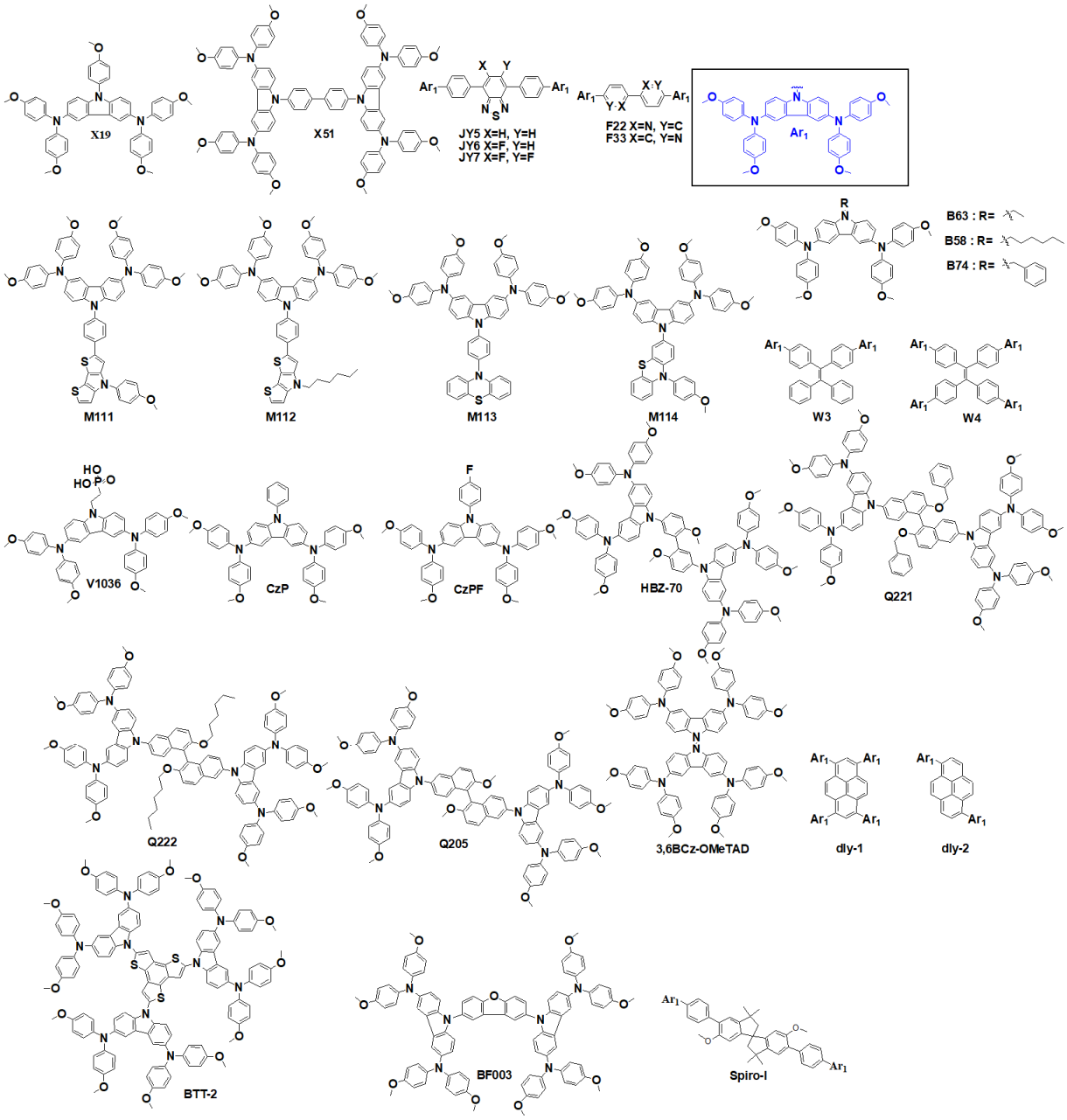
X19
X51
JY5 X=H, Y=H
JY6 X=F, Y=H
JY7 X=F, Y=F
F22 X=N, Y=C
F33 X=C, Y=N
B63 : R=
B58 : R=
B74 : R=
M111
M112
M113
M114
W3
W4
V1036
CzP
CzPF
HBZ-70
Q221
Q222
Q205
3,6BCz-OMeTAD
dly-1
dly-2
BTT-2
BF003
Spiro-I

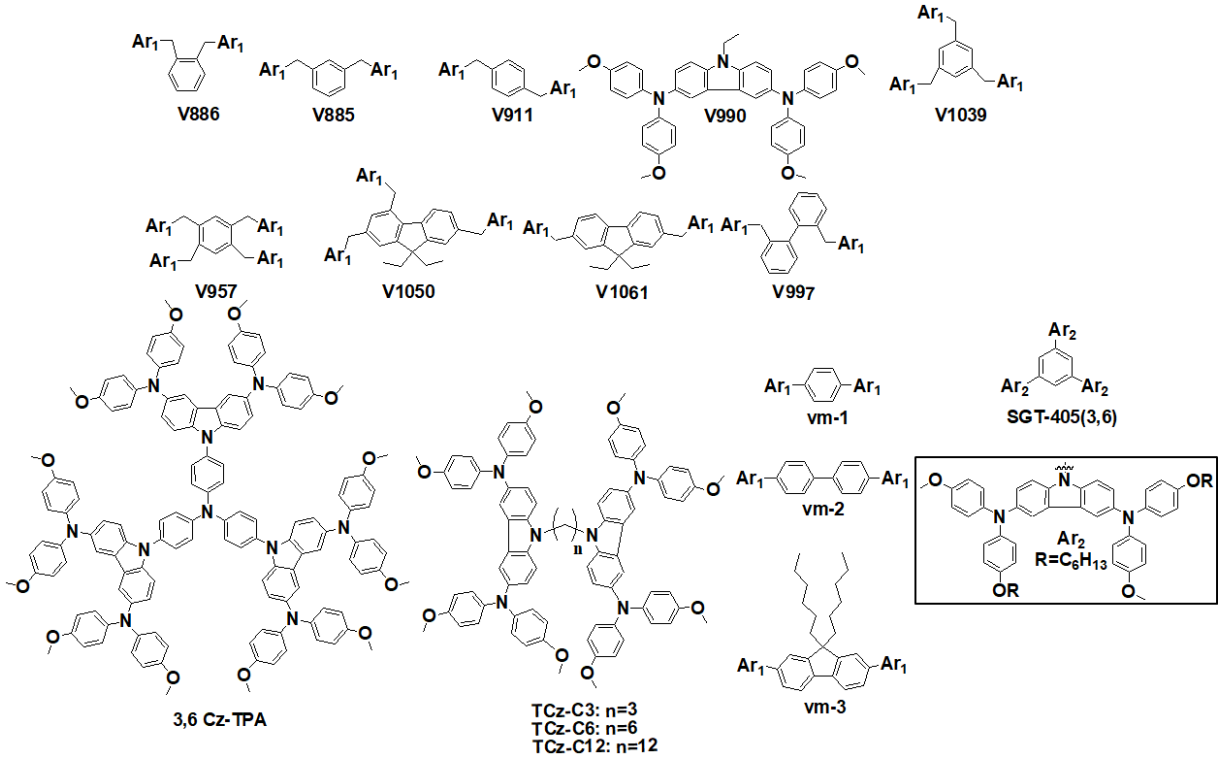

Scheme 4. Chemical structure of HTMs based on 3,6CzDMPA.

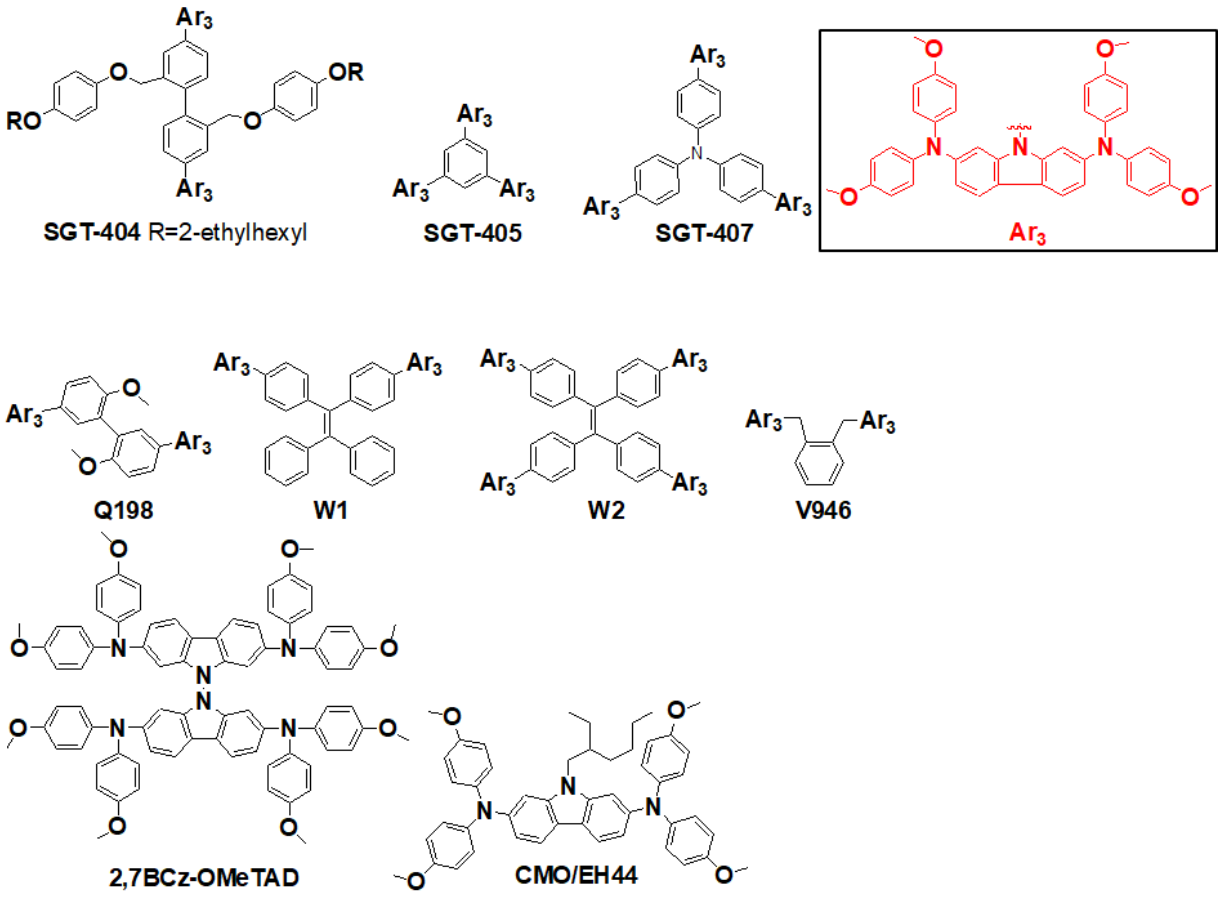

Scheme 5. Chemical structure of HTMs based on 2,7CzDMPA.

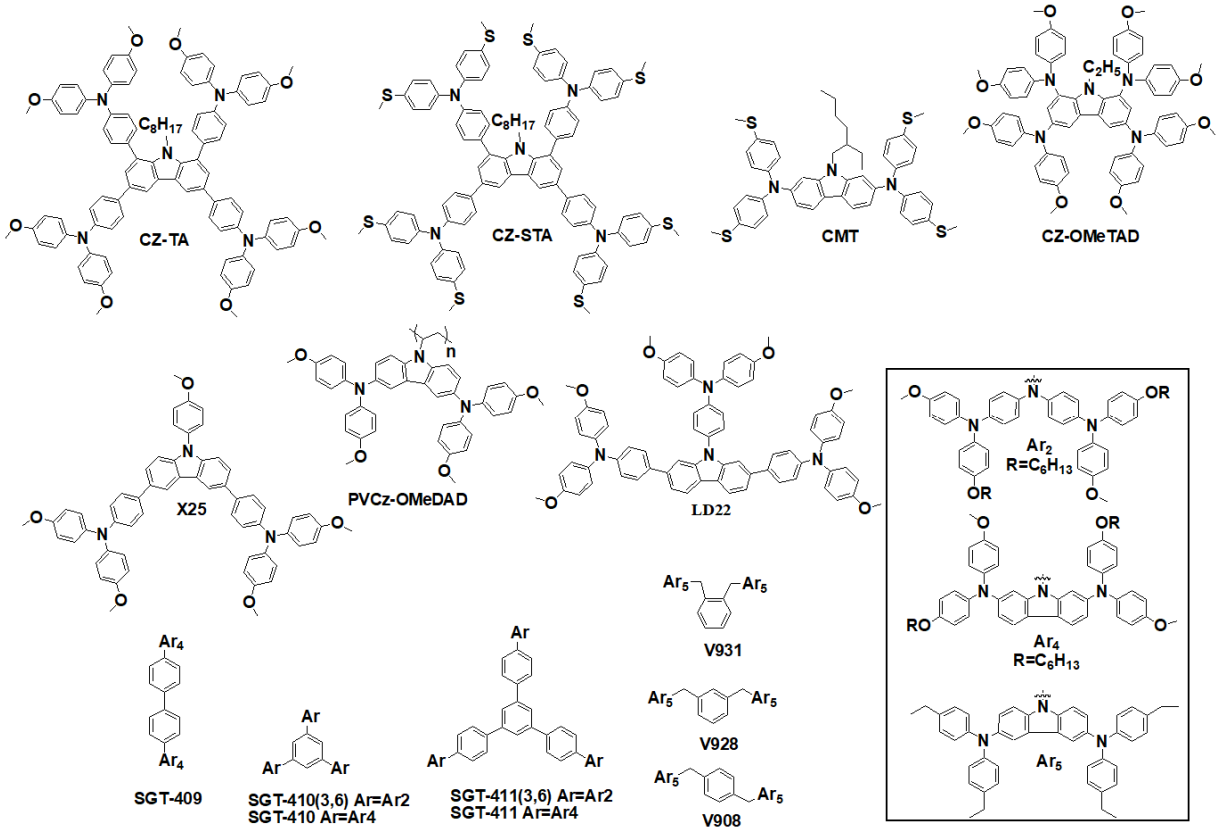

Scheme 6. Chemical structure of HTMs with structural variations derivating from the CzDMPA unit.

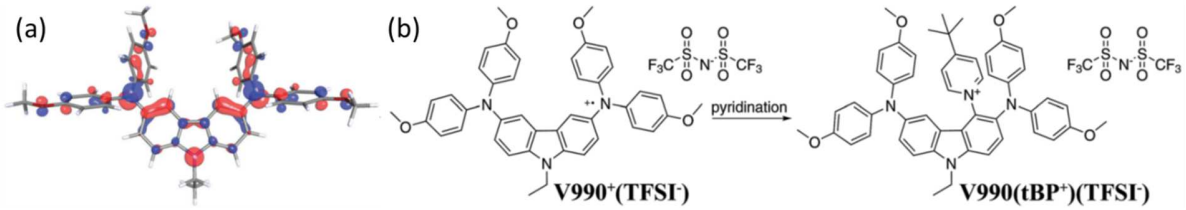

Figure 2. LUMO energy level (a) and reaction scheme of pyridination (b) **V990⁺** radical cation.[99] Reproduced from ref. 99 with permission from the Royal Society of Chemistry, copyright 2018.

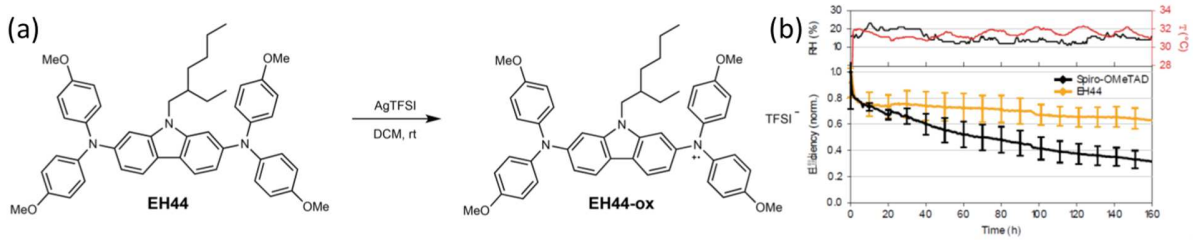

Figure 3. Reaction scheme for the preparation of **EH44-ox** (a), monitoring of relative humidity, temperature and evolution of FTO/TiO_2/$FA_xMA_yCs_{1-x-y}Pb(I_{1-x}Br_z)_3$/HTM/Au devices efficiency tested under illumination (ISOS-L-1 conditions, approximately 77% of 1 sun irradiation) (b).[87] Reproduced from ref. 87 with permission of Nature Research, copyright 2018.

DMPA-containing carbazole-based hole transporting materials for perovskite solar cells: recent advances and perspectives

Nicolas Berton, Rana Nakar, Bruno Schmaltz*

Laboratoire de Physico-Chimie des Matériaux et des Electrolytes pour l'Energie (PCM2E), Université de Tours, Parc de Grandmont, Tours 37200, France

* Corresponding author : bruno.schmaltz@univ-tours.fr

Table 1. Thermal properties and hole mobility data of 3,6CzDMPA compounds.

HTMs	T_g (°C)	T_m (°C)	T_D (°C)	Mobility $cm^2 V^{-1} s^{-1}$	Ref
X19	85	-	392	1.19×10^{-4} [bc]	41
X51	-	-	-	1.51×10^{-4} [bc]	41
X51	-	-	-	1.17×10^{-4} [ac]	64
JY5	165	-	448	3.53×10^{-4} [ac]	64
F22	162	-	442	5.37×10^{-4} [ac]	69
F33	151	-	380	6.79×10^{-4} [ac]	69
JY6	154	-	481	8.84×10^{-4} [ac]	54
JY7	134	-	484	4.28×10^{-4} [ac]	54
Q221	198	-	321	-	63
Q222	128	88	401	-	63
Q205	188	-	> 420	-	61
HBZ-70	167.6	-	418.4	-	62
M111	108.5	-	390.9	1.35×10^{-5} [bc]	55
M112	96.7	-	409.5	2.30×10^{-6} [bc]	55
M113	120.4	-	431.3	7.86×10^{-6} [bc]	55
M114	130.1	-	424.9	4.05×10^{-5} [bc]	55
W4	-	-		1.35×10^{-4} [ac]	50
3.6BCz-OMeTAD	100	-	397	1.13×10^{-4} [bc]	56
dly-1	-	-	> 300	4.59×10^{-4} [ac]	81
dly-2	-	-	> 300	1.42×10^{-3} [ac]	81
BTT-2	216	-	> 400	-	65
BF-003	-	-	400	-	80
Spiro-I	-	-		-	82
V886	141	-	390	6.00×10^{-4} [b,d]	70
V885	139	-	393	4.60×10^{-3} [b,d]	44
V911	139	-	410	1.00×10^{-2} [b,d]	44
V990 / B63	80	-	407	4.80×10^{-5} [b,d]	44
V1039	160	-	414	3.00×10^{-4} [b,d]	44
V957	161	-	419	1.40×10^{-3} [b,d]	44
V1050	166	-	400	1.70×10^{-4} [b,d]	45
V1061	146	-	420	2.00×10^{-4} [b,d]	45
V997	140	-	300	1.30×10^{-4} [b,d]	68
V1036	-	-	343	-	79

CzP	97	-	441	2.70×10^{-6} [b,e]	39,53
CzPF	82	-		5.50×10^{-6} [b,e]	53
3,6Cz-TPA	146	-	432	7.00×10^{-6} [b,e]	67
B63 / V990	80	-	375	1.77×10^{-7} [b,e]	58,59
B58	55	-	398	2.87×10^{-7} [b,e]	58,59
B74	66	-	336	1.18×10^{-7} [b,e]	58,59
TCz-C3	107	-	407	5.40×10^{-6} [b,e]	43
TCz-C6	66	-	401	2.70×10^{-6} [b,e]	43
TCz-C12	47	-	430	1.30×10^{-6} [b,e]	43
Vm-1	186	-	385	-	60
Vm-2	153	-	382	-	60
Vm-3	124	-	383	-	60
SGT-405(3,6)	193	333	396	1.80×10^{-4} [b,c]	66

[a] Doped, [b] Pristine. Hole mobility measured by [c] SCLC, [d] XTOF, and [e] OFET.

Table 2. Photovoltaic characteristics of PSC based on 3,6CzDMPA HTMs (device architecture: mesoporous n-i-p (M), planar n-i-p (P) or inverse planar p-i-n). The PCE of reference devices based on spiro-OMeTAD HTM are indicated for comparison.

HTMs	Perovskite	ETM	Architecture	Dopants	Thickness of HTM layer	Jsc (mA.cm^{-2})	Voc (V)	FF	η (%)	η (%) spiro-OMeTAD	Ref
X19	$MAPbI_{3-x}Cl_X$	TiO_2	M	LiTFSI, tBP	-	17.14	0.76	0.58	7.60	10.20	41
X51	$MAPbI_{3-x}Cl_X$	TiO_2	M	LiTFSI, tBP	-	16.79	0.88	0.66	9.80	10.20	41
X51	$MAPbI_{3-x}Cl_X$	TiO_2	P	LiTFSI, tBP	-	19.50	0.99	0.68	13.20	16.24	64
JY5	$MAPbI_{3-x}Cl_X$	TiO_2	P	LiTFSI, tBP	-	21.06	1.06	0.76	16.87	16.24	64
JY6	$MAPbI_{3-x}Cl_X$	TiO_2	P	LiTFSI, tBP	-	21.39	1.07	0.81	18.54	16.24	54
JY7	$MAPbI_{3-x}Cl_X$	TiO_2	P	LiTFSI, tBP	-	20.58	1.05	0.73	15.71	16.24	54
F22	$MAPbI_{3-x}Cl_X$	TiO_2	P	LiTFSI, tBP	-	21.26	1.05	0.79	17.71	16.24	69
F33	$MAPbI_{3-x}Cl_X$	TiO_2	P	LiTFSI, tBP	-	21.01	1.11	0.79	18.48	16.24	69
Q221	$MAPbI_3$	TiO_2	M	LiTFSI, tBP	-	15.87	0.95	0.67	10.05	10.06	63
Q222	$MAPbI_3$	TiO_2	M	LiTFSI, tBP	-	15.59	0.91	0.61	8.66	10.06	63
Q205	$MAPbI_3$	TiO_2	M	LiTFSI, tBP	-	13.23	0.98	0.50	6.51	8.73	61
HBZ-70	$MAPbI_3$	TiO_2	M	LiTFSI, tBP	310 nm	8.47	1.03	0.52	4.53	5.10	62
M111	$Cs_{0.05}(FA_{0.83}MA_{0.17})_{0.95}Pb(I_{0.83}Br_{0.17})_3$	SnO_2	P	LiTFSI, tBP, FK209	-	21.56	1.02	0.72	15.88	18.07	55
M112	$Cs_{0.05}(FA_{0.83}MA_{0.17})_{0.95}Pb(I_{0.83}Br_{0.17})_3$	SnO_2	P	LiTFSI, tBP, FK209	-	21.56	1.02	0.67	14.72	18.07	55
M113	$Cs_{0.05}(FA_{0.83}MA_{0.17})_{0.95}Pb(I_{0.83}Br_{0.17})_3$	SnO_2	P	LiTFSI, tBP, FK209	-	21.97	1.01	0.67	14.86	18.07	55

M114	$Cs_{0.05}(FA_{0.83}MA_{0.17})_{0.95}Pb(I_{0.83}Br_{0.17})_3$	SnO_2	P	LiTFSI, tBP, FK209	-	22.24	1.06	0.73	17.17	18.07	55
W4	$MAPbI_{3-X}Cl_X$	TiO_2	P	LiTFSI, tBP	-	19.76	0.98	0.69	13.30	15.01	50
3.6B Cz-OMeTAD	$Cs_{0.05}FA_{0.79}MA_{0.16}PbI_{2.49}Br_{0.51}$	TiO_2	M	Dopant free	30 nm	21.34	1.12	0.71	17.00	18.50	56
dly-1	$(FAPbI_3)_{0.75}(MAPbI_3)_{0.17}(MAPbBr_3)_{0.08}$	TiO_2	P	LiTFSI, tBP	-	22.68	0.97	0.78	17.19	19.59	81
dly-2	$(FAPbI_3)_{0.75}(MAPbI_3)_{0.17}(MAPbBr_3)_{0.08}$	TiO_2	P	LiTFSI, tBP	-	23.24	1.04	0.75	18.23	19.59	81
BTT-2	$MAPbI_3$	TiO_2	M	LiTFSI, tBP, FK209	150 nm	20.60	1.09	0.77	17.00	18.10	65
BTT-2	$(MAPbI_3)_{0.15}(MAPbBr_3)_{0.85}$	TiO_2	M	Li-TFSI, tBP, FK209	150 nm	22.30	1.03	0.75	17.50	17.50	65
BF-003	$MAPbI_3$	TiO_2	M	LiTFSI, tBP, FK209	-	21.22	1.03	0.64	14.07	15.04	80
Spiro-I	MAFACsPbIBr	TiO_2		LiTFSI, tBP	63 nm	24.57	1.06	0.71	18.57	19.17	82
V886	$MAPbI_3$	TiO_2	M	LiTFSI, tBP, FK209	-	21.38	1.09	0.73	16.91	18.36	70
V886	$Cs_{0,1}(MA_{0,15}FA_{0,85})_{0,9}Pb(I_{0,85}Br_{0,15})$	TiO_2	M	LiTFSI, tBP, FK209	80 - 150 nm	22.09	1.10	0.75	18.45	18.79	44
V885	$Cs_{0,1}(MA_{0,15}FA_{0,85})_{0,9}Pb(I_{0,85}Br_{0,15})$	TiO_2	M	LiTFSI, tBP, FK209	80 - 150 nm	22.43	1.10	0.76	18.92	18.79	44
V911	$Cs_{0,1}(MA_{0,15}FA_{0,85})_{0,9}Pb(I_{0,85}Br_{0,15})$	TiO_2	M	LiTFSI, tBP, FK209	80 - 150 nm	22.40	1.10	0.76	18.86	18.79	44

V931	$Cs_{0,1}(MA_{0,15}FA_{0,85})_{0,9}Pb(I_{0,85}Br_{0,15})$	TiO_2	M	LiTFSI, tBP, FK209	80 - 150 nm	21.02	1.07	0.71	16.30	18.79	44
V928	$Cs_{0,1}(MA_{0,15}FA_{0,85})_{0,9}Pb(I_{0,85}Br_{0,15})$	TiO_2	M	LiTFSI, tBP, FK209	80 - 150 nm	21.83	1.03	0.73	16.54	18.79	44
V908	$Cs_{0,1}(MA_{0,15}FA_{0,85})_{0,9}Pb(I_{0,85}Br_{0,15})$	TiO_2	M	LiTFSI, tBP, FK209	80 - 150 nm	21.31	1.04	0.73	16.35	18.79	44
V990	$Cs_{0,1}(MA_{0,15}FA_{0,85})_{0,9}Pb(I_{0,85}Br_{0,15})$	TiO_2	M	LiTFSI, tBP, FK209	80 - 150 nm	12.58	0.94	0.42	5.02	18.79	44
V1039	$Cs_{0,1}(MA_{0,15}FA_{0,85})_{0,9}Pb(I_{0,85}Br_{0,15})$	TiO_2	M	LiTFSI, tBP, FK209	80 - 150 nm	22.10	1.05	0.72	16.84	18.79	44
V957	$Cs_{0,1}(MA_{0,15}FA_{0,85})_{0,9}Pb(I_{0,85}Br_{0,15})$	TiO_2	M	LiTFSI, tBP, FK209	80 - 150 nm	22.12	1.04	0.72	16.78	18.79	44
V1050	$FA_{0.83}Cs_{0.17}Pb(I_{0.8}Br_{0.2})_3$	SnO_2	P	LiTFSI, tBP, Co[t-BuPyPz]3[TFSI]3	-	22.00	1.05	0.79	18.30	18.90	45
V1061	$FA_{0.83}Cs_{0.17}Pb(I_{0.8}Br_{0.2})_3$	SnO_2	P	LiTFSI, tBP, Co[t-BuPyPz]3[TFSI]3	-	21.60	0.96	0.79	16.70	18.90	45
V997	$FA_{0.83}Cs_{0.17}Pb(I_{0.8}Br_{0.2})_3$	TiO_2	P	LiTFSI, tBP, Co[t-BuPyPz]$_3$[TFSI]$_3$	-	20.60	1.07	0.75	17.50	17.50	68
V997	$MAPbI_3$	TiO_2	P	LiTFSI, tBP	-	20.50	1.00	0.63	13.00	13.50	68
V1036	$Cs_{0,5}(MA_{0,17}FA_{0,85})_{0,9}$	-	p-i-n	-	-	21.01	1.00	0.78	16.46	17.69*	79

	$Pb(I_{0,85}Br_{0,15})$										
CzP	$MAPbI_3$	TiO_2/PCBM	P	LiTFSI, tBP	-	18.22	1.04	0.69	13.08	13.45	53
CzPF	$MAPbI_3$	TiO_2/PCBM	P	LiTFSI, tBP	-	17.31	1.03	0.7	12.41	13.45	53
3,6Cz-TPA	$(FAPbI_3)_{0.85}(CsPbBr_3)_{0.15}$	TiO_2	M	LiTFSI, tBP	-	21.98	1.00	0.72	15.89	17.13	67
B63	$MAPbI_3$	TiO_2	M	LiTFSI, tBP	100 nm	18.6	0.87	0.59	10.8	11.2	58
B58	$MAPbI_3$	TiO_2	M	LiTFSI, tBP	100 nm	13.7	0.83	0.59	7.5	11.2	58
B74	$MAPbI_3$	TiO_2	M	LiTFSI, tBP	100 nm	17.5	0.93	0.54	9.9	11.2	58
SGT-405(3,6)	$MAPbCl_{3-x}I_x$	TiO_2	M	LiTFSI, tBP, FK209	-	22.92	1.04	0.78	18.87	17.71	66

*Using PTAA as reference HTM instead of spiro-OMeTAD.

Table 3. Thermal properties and mobility data of 2,7CzDMPA compounds.

HTMs	T_g (° C)	T_m (° C)	T_D (° C)	Mobility $cm^2 V^{-1} s^{-1}$	Ref
SGT-404	70.5	-	330	-	52
SGT-405	~200	327.6	> 400	$1.05x10^{-4}$ [b,c]	52,66
SGT-407	170.8	-	> 400	-	52
Q197	168	-	> 420	-	61
Q198	157	-	> 420	-	61
W1	-	-	-	$2.74x10^{-14}$ [a,c]	50
W2	-	-	-	$3.06x10^{-4}$ [a,c]	50
V946	113	-	411	$6.50x10^{-4}$ [b,d]	44
2.7 BCz-OMeTAD	145	-	442	$0.95x10^{-4}$ [b,c]	56
CMO/EH44	-	-	325	$1.40x10^{-5}$ [b,c]	86,87

[a]Doped, [b] Pristine. Hole mobility measured by [c] SCLC, [d] XTOF.

Table 4. Photovoltaic characteristics of PSC based on 2,7CzDMPA HTMs (device architecture: mesoporous (M) or planar (P) n-i-p). The PCE of reference devices based on spiro-OMeTAD HTM are indicated for comparison.

HTMs	Perovskite	ETL	Dopants	Architecture	Thickness of HTM layer	Jsc (mA. cm^{-2})	Voc (V)	FF	η (%)	η (%) spiro-OMeTAD	Ref
SGT-404	$MAPbI_3$	TiO_2	LiTFSI, tBP, FK209 Co(III) TFSI	M	250 nm	19.76	0.96	0.70	13.28	15.23	52
SGT-405	$MAPbI_3$	TiO_2	LiTFSI, tBP, FK209 Co(III) TFSI	M	300 nm	20.28	1.02	0.71	14.79	15.23	52
SGT-405	$MAPbCl_{3-x}I_x$	TiO_2	LiTFSI, tBP, FK209	M		22.32	1.05	0.76	18.00	17.71	66
SGT-407	$MAPbI_3$	TiO_2	LiTFSI, tBP, FK209 Co(III) TFSI	M	230 nm	20.35	0.99	0.69	13.86	15.23	52
Q197	$MAPbI_3$	TiO_2	LiTFSI, tBP	M		16.53	0.90	0.56	8.38	8.73	61
Q198	$MAPbI_3$	TiO_2	LiTFSI, tBP	M		16.69	0.86	0.49	7.08	8.73	61
W1	$MAPbI_{3-x}Cl_X$	TiO_2	LiTFSI, tBP	P		21.55	1.01	0.69	14.92	15.01	50
W2	$MAPbI_{3-x}Cl_X$	TiO_2	LiTFSI, tBP	P		22.23	1.02	0.74	16.74	15.01	50
V946	$Cs_{0,1}(MA_{0,15}FA_{0,85})_{0,9}Pb(I_{0,85}Br_{0,15})$	TiO_2	LiTFSI, tBP, FK209	M	80 -150 nm	21.86	1.06	0.73	17.02	18.79	44
2.7 BCz-OMeTAD	$Cs_{0.05}FA_{0.79}MA_{0.16}PbI_{2.49}Br_{0.51}$	TiO_2	Dopant free	M	30 nm	22.38	1.09	0.73	17.60	18.50	56
CMO	$MAPbI_3$	TiO_2	Dopant free	P	50 nm	25.19	0.93	0.67	15.92	16.70	86
EH44	$(FA_{0.76}MA_{0.21}Cs_{0.03})_{0.67}Pb(I_{0.89}Br_{0.11})_{2.5}$	TiO_2	14wt% EH44-ox, tBP	M	60 nm	21.71	1.09	0.77	18.50	19.60	87

Table 5. Thermal properties and mobility data of CzDMPA derivative HTMs.

HTMs	T_g (°C)	T_m (°C)	T_D (°C)	Mobility $cm^2 V^{-1} s^{-1}$	Ref
CZ-TA	192	-	421	1.65×10^{-4} [b,c]	91
CMT	-	-	387	2.60×10^{-5} [b,c]	93
CZ-STA	110.2	-	401	-	92
CZ-TA;CZ-STA 90:10	-	-	-	2.00×10^{-4} [a,c]	92
Cz-OMeTAD	114.9	-	423	1.82×10^{-3} [b,c]	88
X25	-	-		-	89
PVCz-OMeDAD	229	-	418	3.44×10^{-4} [b,c]	94
LD22	132	-	-	1.65×10^{-5} [a,c]	90
SGT-409	83	-	> 400	-	51
SGT-410	70	-	> 400	-	51
SGT-411	-	218	> 400	-	51
SGT-410(3,6)	-	-	372	5.27×10^{-5} [b,c]	66
SGT-411(3,6)	-	-	372	8.74×10^{-5} [b,c]	66
V931	158	233	401	7.80×10^{-4} [b,d]	44
V928	151	-	414	3.70×10^{-4} [b,d]	44
V908	163	337	420	4.00×10^{-4} [b,d]	44

[a]Doped, [b] Pristine. Hole mobility measured by [c] SCLC, [d] XTOF.

Table 6. Photovoltaic characteristics of PSC based on HTMs derivating from the CzDMPA structure (device architecture: mesoporous (M) or planar (P) n-i-p). The PCE of reference devices based on spiro-OMeTAD HTM are indicated for comparison.

HTMs	Perovskite	ETL	Architecture	Dopants	Thickness of HTM layer	Jsc (mA. cm^{-2})	Voc (V)	FF	η (%)	η (%) spiro-OMeTAD	Ref
CZ-TA	$MA_{0.7}FA_{0.3}PbI_3$	SnO_2/C_{60}-SAM	P	LiTFSI, tBP	50 nm	21.66	1.04	0.81	18.32	18.28	91
CMT	$MAPbI_3$	compact-TiO_2	P	Dopant Free	-	21.82	1.03	0.58	13.05	-	93
CMT	$MAPbI_3$	compact-TiO_2	P	LiTFSI, tBP	-	20.79	0.98	0.51	10.55	16.70	93
CZ-STA	$MA_{0.7}FA_{0.3}PbI_3$	SnO_2/C_{60}-SAM	P	LiTFSI, tBP	50 nm	21.96	1.05	0.70	16.21	18.28	92
CZ-TA;CZ-STA 90:10	$MA_{0.7}FA_{0.3}PbI_3$	SnO_2/C_{60}-SAM	P	LiTFSI, tBP	50 nm	22.51	1.08	0.82	19.85	18.28	92
Cz-OMeTAD	$MAPbI_3$	SnO_2	P	LiTFSI	150 nm	22.26	1.14	0.71	17.81	18.59	88
X25	$FA_{0.85}MA_{0.15}Pb(I_{0.85}Br_{0.15})_3$	TiO_2	M	-	-	22.50	1.10	0.70	17.40	-	89
PVCz-OMeDAD	$FA_{0.85}MA_{0.15}Pb(I_{0.85}Br_{0.15})_3$	TiO_2	M	Dopant Free	30 nm	21.93	1.08	0.67	16.09	9.62	94
LD22	$(FAPbI_3)_{0.85}(MAPbBr_3)_{0.15}$	TiO_2	M	Dopant Free	-	19.60	1.03	0.65	13.04	17.73	90
LD22	$(FAPbI_3)_{0.85}(MAPbBr_3)_{0.15}$	TiO_2	M	LiTFSI, tBP and FK209	-	21.12	1.06	0.77	17.18	17.73	90
SGT-409	$MAPbI_3$	TiO_2	M	LiTFSI, tBP, FK209	-	18.63	0.94	0.62	10.96	13.76	51

SGT-410	$MAPbI_3$	TiO_2	M	LiTFSI, tBP, FK209	-	18.55	0.98	0.67	12.61	13.76	51
SGT-411	$MAPbI_3$	TiO_2	M	LiTFSI, tBP, FK209	-	18.60	1.00	0.67	13.00	13.76	51
SGT-410(3,6)	$MAPbCl_{3-x}I_x$	TiO_2	M	LiTFSI, tBP, FK209	-	20.57	1.04	0.75	16.20	17.71	66
SGT-411(3,6)	$MAPbCl_{3-x}I_x$	TiO_2	M	LiTFSI, tBP, FK209	-	21.19	1.03	0.75	16.50	17.71	66
V931	$Cs_{0,1}(MA_{0,15}FA_{0,85})_{0,9}Pb(I_{0,85}Br_{0,15})$	TiO_2	M	LiTFSI, tBP, FK209	80 - 150 nm	21.02	1.07	0.71	16.30	18.79	44
V928	$Cs_{0,1}(MA_{0,15}FA_{0,85})_{0,9}Pb(I_{0,85}Br_{0,15})$	TiO_2	M	LiTFSI, tBP, FK209	80 - 150 nm	21.83	1.03	0.73	16.54	18.79	44
V908	$Cs_{0,1}(MA_{0,15}FA_{0,85})_{0,9}Pb(I_{0,85}Br_{0,15})$	TiO_2	M	LiTFSI, tBP, FK209	80 - 150 nm	21.31	1.04	0.73	16.35	18.79	44